1971

The radiation patterns and current distribution of two arbitrary size coaxial circular loop antennas

Corcoran, Joseph Francis

Monterey, California; Naval Postgraduate School

THE RADIATION PATTERNS AND CURRENT DISTRIBUTIONS OF TWO ARBITRARY SIZE COAXIAL CIRCULAR LOOP ANTENNAS

Joseph Francis Corcoran

United States
Naval Postgraduate School

THESIS

The Radiation Patterns and Current Distributions of Two Arbitrary Size Coaxial Circular Loop Antennas

by

Joseph Francis Corcoran

Thesis Advisor: Richard W. Adler

June 1971

Approved for public release; distribution unlimited.

The Radiation Patterns and Current Distributions of Two Arbitrary Size Coaxial Circular Loop Antennas

by

Joseph Francis Corcoran
Lieutenant Commander, United States Navy
B.S., United States Naval Academy, 1962

Submitted in partial fulfillment of the
requirements for the degree of

MASTER OF SCIENCE IN ELECTRICAL ENGINEERING

from the

NAVAL POSTGRADUATE SCHOOL
June 1971

ABSTRACT

For many years the cylindrical dipole and circular loop have been thought of as the basic radiating elements. Due to its relative simplicity the study of the cylindrical dipole is quite complete, but owning to the degree of complexity, progress in the theory of the loop has been much slower. In recent years the isolated circular loop antenna of arbitrary size has been the subject of mathematical and experimental analysis [7], [6]. It was not until 1970 that the first complete and general mathematical solution for the mutual admittance of two arbitrary size coaxial circular loop antennas was published. The problem was formulated by Adler in terms of coupled integral equations for the current distributions on the loops [1]. The equations were solved using the Fourier series representation of the current distributions. The study presented here is the next logical step beyond the work of Adler. Using his current equations the current distributions are calculated at each point around the two loops. The input admittance, electric field and power gains are calculated. Radiation patterns and the loop current distributions are plotted for two cases: (1) both loops driven and (2) one loop acting as a short circuited parasite.

TABLE OF CONTENTS

LIST OF ILLUSTRATIONS

ACKNOWLEDGEMENTS

The author is grateful to Dr. Richard W. Adler for the inspiration to attempt this study and for the many hours of consultation and instruction he rendered so enthusiastically.

All computer calculations were conducted at the W. R. Church Computer Center. The cooperation of the Computer Center staff is appreciated.

I. INTRODUCTION

A. HISTORY OF WORK ON THE LOOP ANTENNA PROBLEM.

In 1897 Pocklington excited a thin loop by a plane wave and obtained a solution for the induced current in the form of a Fourier series expansion [9]. Hallen continued the work by producing an expression for the current distribution in the driven case [3]. Due to singularities arising in the Fourier series coefficients, Hallen's technique applied only to electrically small loops. Storer attempted to surmount the limitations of Hallen's work and derive an expression for the current in the case of a large loop [10]. He expressed the series in integral form and evaluated the integral in the sense of the Cauchy principal value. Experiments of Kennedy showed Storer's calculations produced an unacceptable deviation between calculated and measured susceptance [6]. Wu reviewed the work of Hallen and Storer and discovered that the shortcomings arose from over-simplifying the problem [11]. That is they assumed the electric field intensity on the surface of the conductor was uniform around the circumference with a filamentary current flowing at the center of the conductor.

Wu then modified Storer's solution by changing the one dimensional integral equations to two dimensional integral equations in order to account for the electric field variation around the circumference of the conductor. Wu assumed a longitudinal current flow on the surface of the conductor and allowed no circumferential component. He showed this to be equivalent to a uniformly distributed current density on the cross section of the conductor, which allowed the current to be treated

as filamentary and concentrated at the center of the conductor. After this simplification the equations were again one dimensional but no longer required uniform electric field around the circumference. King applied Wu's modification to calculate the admittance of a single loop [7]. This proved Storer's work to be valid but only for the case of small loops.

The first attempt at solving the multi-loop problem was by Iizuka for the special case of two identical loops [5]. In 1970 Adler advanced King's work by devising a completely general mathematical solution to the mutual admittance of large arbitrary size coaxial loops. Adler also measured the admittance in the two-loop case and found close agreement with theoretical values [1].

B. SCOPE AND LIMITATIONS OF THE STUDY

This paper completes the study of large arbitrary size coaxial loop antenna arrays. Current distributions and radiation patterns are calculated and plotted for various array geometries. Although only the two-loop situation is presented herein, the theory applies to the n-loop situation as well. Since the ϕ (polarized) mode electric field component is of primary interest, this mode is examined in detail. The θ mode is calculated and one representative field pattern is plotted. The range of loop dimensions selected is for the resonant and near resonant case. a, b, and c are the conductor radius, loop radius and loop spacing respectively; the range of parameters are expressed as

$$0.5 \leq kb \leq 2.0, \qquad 0.5 \leq kc \leq 7.0$$

where:

$$k = \frac{2\pi}{\lambda} .$$

ka is determined by the thickness parameter:

$\Omega = 2 \ln \frac{2\pi b}{a}$ and λ is the wave length.

Having $7.5 \leq \Omega \leq 15$ represents a ratio of b/a from approximately 10 to 300. The above parameter limitations are a result of the approximations used in the theoretical analysis of the Fourier coefficients of the current distributions.

Although perfect conductors in free space are specified, the effect of lossy media can be included merely by considering the propagation constant complex. The loops are driven by delta function voltage generators, symbolized by $V\ \delta(\phi)$. The two coupled antennas are treated as a two-port network and conventional circuit analysis techniques are employed to produce a convenient matrix of equations.

II. THEORY

The conductor radius is assumed to be small relative to the loop radius, which allows the current density in each loop, $I_1(\phi)$ and $I_2(\phi)$, to be approximated by an equivalent one-dimensional filamentary current distribution at the center of the loop. The electric field is derived by the scalar and vector potential in terms of the distribution of the current. Readers are referred to Adler's work for the mathematical details of the current equation formulation. Only an outline of the solution is presented here.

As shown in Figure 1, the cylindrical coordinates for points on loops 1 and 2 are (b_1, ϕ', o) and (b_2, ϕ, c) respectively. The angle ϕ' represents the coordinate of the current element, while the angle ϕ represents the electric field observation point coordinate. The distance from the source current element on one loop to the electric field observation point on the other loop is:

$$R_{12} = R_{21} = \sqrt{(b_1-b_2)^2 + c^2 + 4b_1b_2\sin^2\left(\frac{\phi-\phi'}{2}\right)}\ .$$

The distance from one point to another on loop 1 is:

$$R_{11} = \sqrt{4b_1^2\sin^2\left(\frac{\phi-\phi'}{2}\right) + 4a_1^2\sin^2\left(\frac{\psi}{2}\right)},$$

as shown in Figure 2. The same expression applies to loop 2 if the subscript 1 is changed to 2. ψ is the angular distance around the circumference of the conductor surface. In order to simply the notation in this development, the notation for harmonic time variation, $e^{j\omega t}$ has been suppressed.

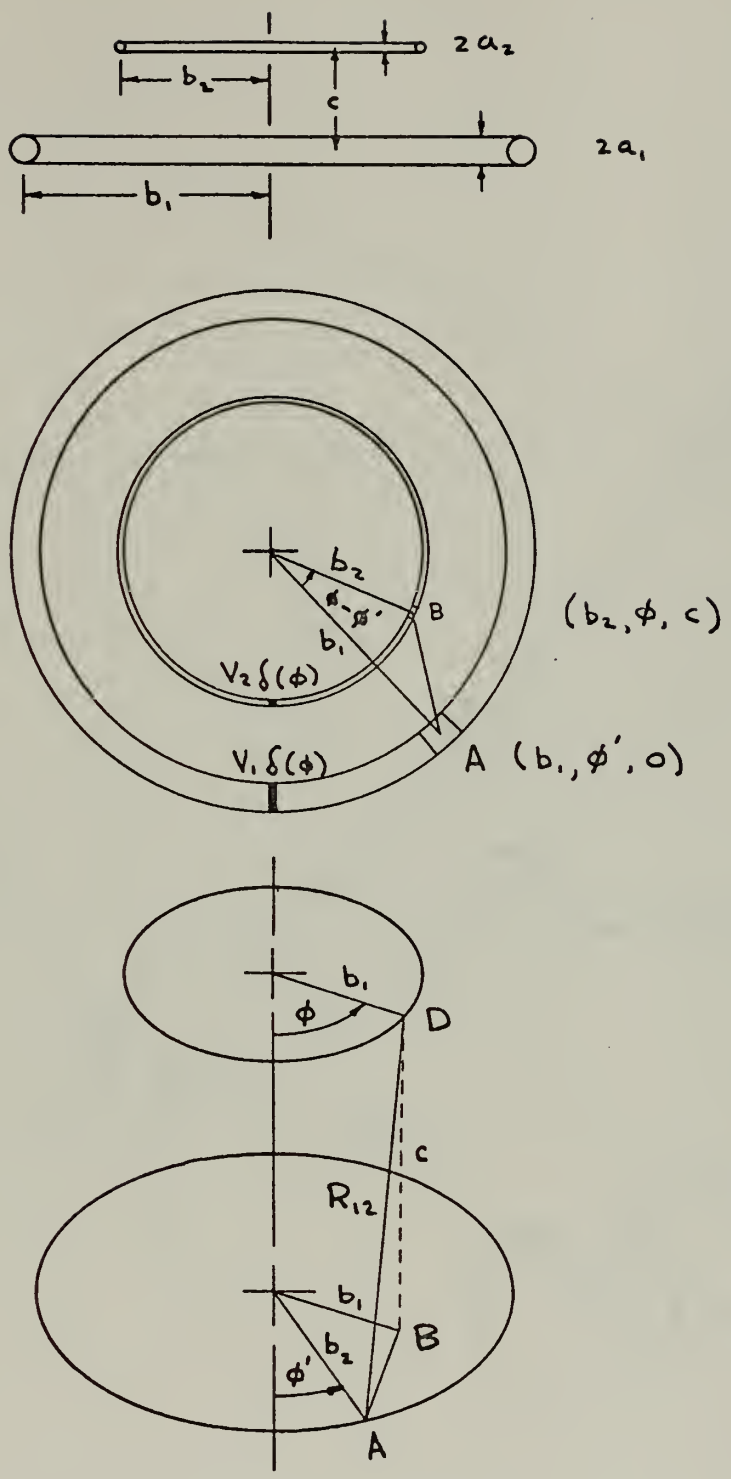

Figure 1. Geometry of Two Unequal Loops

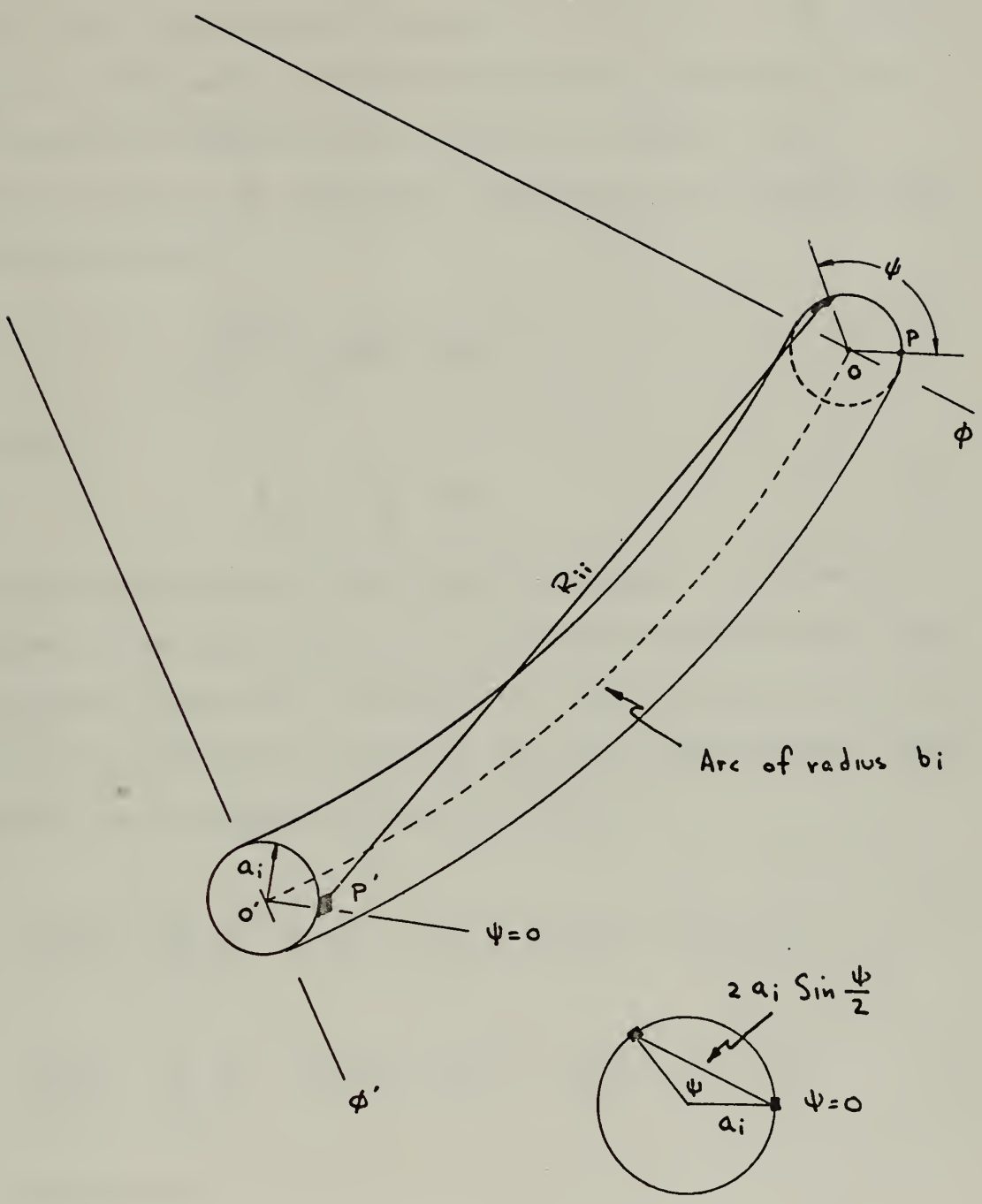

Figure 2. Geometry of Points on a Loop

ε is the total electric field at a point due to loop currents $I_1(\phi)$ and $I_2(\phi)$. The boundary conditions on ε at the conductor surface require the tangential component E_ϕ to be zero at the surface; since no circumferential current is assumed, the E_ϕ component is the only tangential component present. The delta function driving generator placed in the loop causes a singularity in the electric field at the gap such that:

$$\int_{-\pi}^{\pi} E_{\phi_1} b_1 d\phi = -V_1$$

and hence:

$$E_{\phi_1} = -\frac{V_1}{b_1}\ \delta(\phi) \tag{1}$$

The boundary conditions on both loops are analogous. ε_ϕ is the ϕ component of the total electric field due to the currents on both loops. These boundary conditions, when applied to the expressions for the total electric field intensity, specify the following coupled complex integral equations for the unknown current distributions:

$$V_1 \delta(\phi) = \frac{jn_o}{4\pi}\int_{-\pi}^{\pi} [K_{11}(\phi-\phi')I_1(\phi') + K_{12}(\phi-\phi')I_2(\phi')]d\phi' \tag{2}$$

$$V_2 \delta(\phi) = \frac{jn_o}{4\pi}\int_{-\pi}^{\pi} [K_{21}(\phi-\phi')I_1(\phi') + K_{22}(\phi-\phi')I_2(\phi')]d\phi' \tag{3}$$

In these equations

$$K_{ij}(\phi-\phi') = [kb_i b_j \cos(\phi-\phi') + \frac{1}{k}\ \frac{\partial^2}{\partial\phi^2}\ ]\ W_{ij}(\phi-\phi') \tag{4}$$

where K_{ij} is the kernel of the integral equations and

$$[kb_i b_j \cos(\phi-\phi') + \frac{1}{k}\frac{\partial^2}{\partial\phi^2}]$$

operates on $W_{ij}(\phi-\phi')$. Wu's contribution to the solution resulted in integrating the term:

$$\frac{e^{-jkR_{ii}}}{R_{ii}} \text{ to get: } W_{ii}(\phi-\phi') = \frac{1}{2\pi}\int_{-\pi}^{\pi} \frac{e^{-jkR_{ii}}}{R_{ii}}\, d\psi \tag{5}$$

where $W_{ii}(\phi-\phi')$ is the Fourier coefficient of:

$$\frac{e^{-jkR_{ii}}}{R_{ii}} \quad . \qquad \text{When } i \neq j$$

$$W_{ij}(\phi-\phi') = \frac{e^{-jkR_{ij}}}{R_{ij}} \quad . \tag{6}$$

n_o is the characteristic impedence of free space.

Equations (2) and (3) are now solved for $I_1(\phi)$ and $I_2(\phi)$ by the orthogonal expansion technique. The kernels of the integral equations and the currents are specified in terms of their respective Fourier series as follows:

$$I_i(\phi) = \sum_{n=-\infty}^{\infty} I_n^i\, e^{-jn\phi'} \tag{7}$$

$$K_{ij}(\phi-\phi') = \sum_{n=-\infty}^{\infty} \alpha_n^{ij}\, e^{-jn(\phi-\phi')} \tag{8}$$

By applying equations (7) and (8) to equations (2) and (3), interchanging the order of integration and summation and performing the integration over ϕ, equations (9) and (10) are formed:

$$j\frac{n_o}{2}\sum_n [\alpha_n^{11} I_n^1 + \alpha_n^{12} I_n^2]\, e^{jn\phi} = V_1\delta(\phi) \tag{9}$$

$$j\frac{n_o}{2}\sum_n [\alpha_n^{21} I_n^1 + \alpha_n^{22} I_n^2]\, e^{jn\phi} = V_2\delta(\phi) \quad . \tag{10}$$

After multiplying both equations by $e^{-jn\phi}$ and integrating over ϕ from $-\Pi$ to Π, the following simultaneous equations are obtained:

$$\begin{vmatrix} \alpha_n^{11} & \alpha_n^{12} \\ \alpha_n^{21} & \alpha_n^{22} \end{vmatrix} \begin{vmatrix} I_n^1 \\ I_n^2 \end{vmatrix} = \frac{1}{j\Pi n_o} \begin{vmatrix} V_1 \\ V_2 \end{vmatrix} . \tag{11}$$

Equations (11) are solved for I_n^1 and I_n^2 and substituted back into equation (7) to get:

$$I_1(\phi) = \frac{1}{j\Pi n_o}\sum_n \cos n\phi \frac{\begin{vmatrix} V_1 & \alpha_n^{12} \\ V_2 & \alpha_n^{22} \end{vmatrix}}{\begin{vmatrix} \alpha_n^{11} & \alpha_n^{12} \\ \alpha_n^{21} & \alpha_n^{22} \end{vmatrix}} e^{-jn\phi} \tag{12}$$

and

$$I_2(\phi) = \frac{1}{j\Pi n_o}\sum_n \cos n\phi \frac{\begin{vmatrix} \alpha_n^{11} & V_1 \\ \alpha_n^{21} & V_2 \end{vmatrix}}{\begin{vmatrix} \alpha_n^{11} & \alpha_n^{12} \\ \alpha_n^{21} & \alpha_n^{22} \end{vmatrix}} e^{-jn\phi} . \tag{13}$$

The task now is to evaluate the α_n^{ij}'s. The coefficients α_n^{ij} are put in terms of the Fourier coefficients κ_n^{ij} of $W_{ij}(\phi-\phi')$ by letting:

$$W_{ij}(\phi-\phi') = \sum_{n=-\infty}^{\infty} \kappa_n^{ij} \, e^{-jn(\phi-\phi')} \tag{14}$$

where:

$$\kappa_n^{ij} = \kappa_{-n}^{ij} = \frac{1}{2\Pi} \int_{-\Pi}^{\Pi} W_{ij}(\phi-\phi') \, e^{jn(\phi-\phi')} \, d\phi. \tag{15}$$

The following difference relationship is arrived at after differentiation of equation (15):

$$\alpha_n^{ij} = \alpha_{-n}^{ij} = \frac{kb_ib_j}{2} \left[\kappa_{n+1}^{ij} + \kappa_{n-1}^{ij} \right] - \frac{n^2}{k} \kappa_n^{ij} \tag{16}$$

$$\alpha_o = kb_ib_j \, \kappa_1^{ij}. \tag{17}$$

For the evaluation of κ_n^{ij} refer to appendix A.

The coordinate system is as indicated in Figure 3. The expressions for the far-zone electric field and gain are developed around Adler's coupled current equations (12) and (13) rewritten below:

$$I_1(\phi) = \frac{1}{j\Pi n_o} \left[\frac{\begin{vmatrix} V_1 & \alpha_o^{12} \\ V_2 & \alpha_o^{22} \end{vmatrix}}{\alpha_o^{11} \alpha_o^{22} - \alpha_o^{12} \alpha_o^{21}} + 2 \sum_{n=1}^{\infty} \cos(n\phi) \, \frac{\begin{vmatrix} V_1 & \alpha_n^{12} \\ V_2 & \alpha_n^{22} \end{vmatrix}}{\alpha_n^{11} \alpha_n^{22} - \alpha_n^{12} \alpha_n^{21}} \right] \tag{18}$$

$$I_2(\phi) = \frac{1}{j\Pi n_o} \left[\frac{\begin{vmatrix} \alpha_o^{11} & V_1 \\ \alpha_o^{21} & V_2 \end{vmatrix}}{\alpha_o^{11} \alpha_o^{22} - \alpha_o^{12} \alpha_o^{21}} + 2 \sum_{n=1}^{\infty} \cos(n\phi) \, \frac{\begin{vmatrix} \alpha_n^{11} & V_1 \\ \alpha_n^{21} & V_2 \end{vmatrix}}{\alpha_n^{11} \alpha_n^{22} - \alpha_n^{12} \alpha_n^{21}} \right]. \tag{19}$$

Let $I_1(\phi)$, the current in loop 1 conductor element b $d\phi'$ at the angle ϕ' be as given in (18) above and $I_2(\phi)$ be the same except for loop 2.

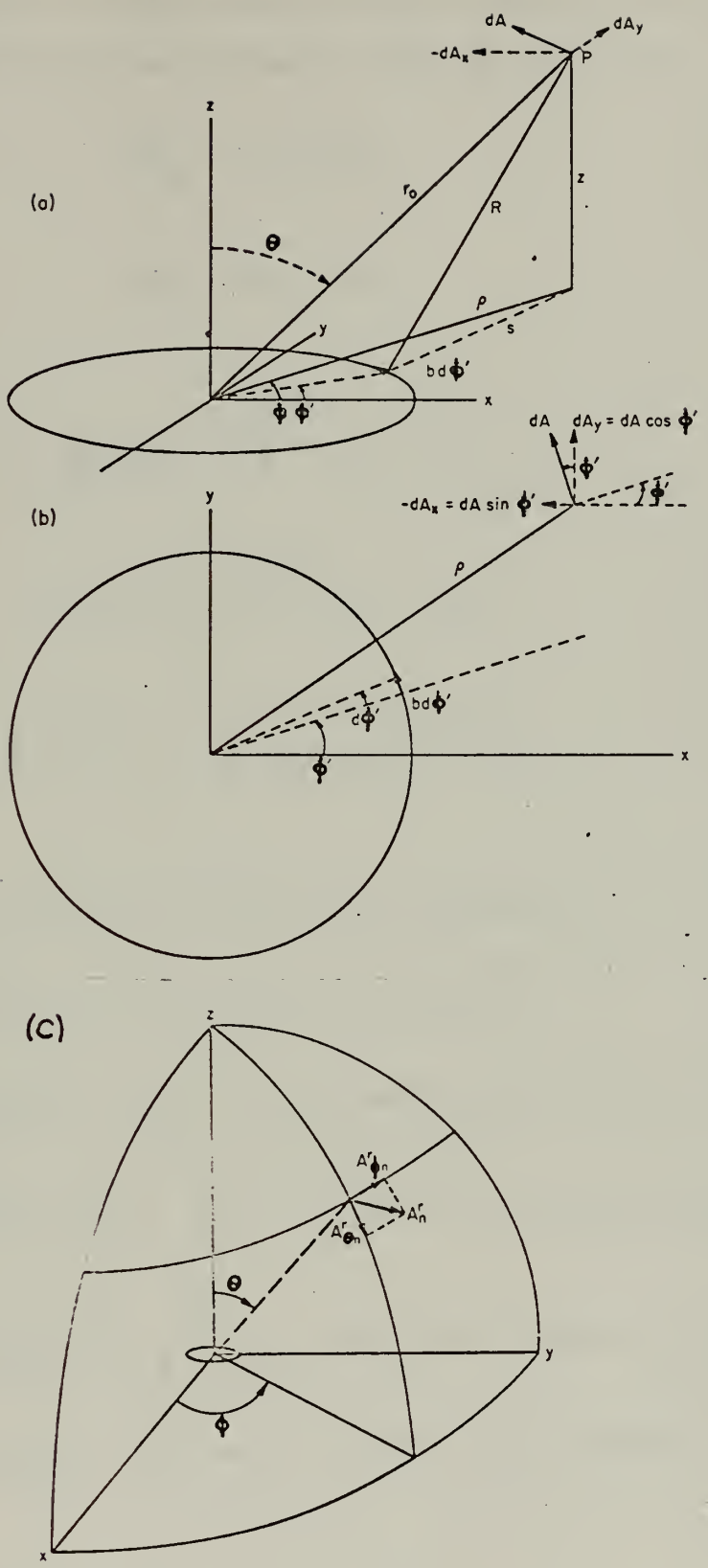

Figure 3. Vector potential for one loop due to element of current $I(\phi')\ b\ d\phi'$ (a) at arbitrary point and (b) at point in plane of loop; (c) spherical coordinates.

The element of vector potential dA_1 at the point (x,y,z) due to $I_1(\phi')$ is composed of two components, dA_{1x} and dA_{1y} where:

$$dA_{1x} = -dA_1 \sin \phi' \tag{20}$$

and

$$dA_{1y} = +dA_1 \cos \phi'. \tag{21}$$

So that:

$$dA_{1x} = - \frac{\mu}{4\pi} I_1(\phi') \frac{e^{-jkR}}{R} \sin \phi' \, b_1 d\phi' \tag{22}$$

and

$$dA_{1y} = + \frac{\mu}{4\pi} I_1(\phi') \frac{e^{-jkR}}{R} \cos \phi' \, b_1 d\phi' \tag{23}$$

where

$$R = \sqrt{z^2 + s^2} = \sqrt{(r_o \cos \theta)^2 + s^2} \tag{24}$$

and

$$s^2 = (r_o \sin \theta)^2 + b^2 - 2br_o \sin \theta \cos (\phi - \phi') . \tag{25}$$

When $b^2 << r_o^2$, $R \simeq r_o - b \sin \theta \cos (\phi - \phi')$.

The vector potential from loop 1 at points where $b^2 << r_o^2$ is thus given by:

$$A_{1x}^r = - \frac{b_1 \mu}{4\pi} \frac{e^{-jkr_o}}{r_o} \int_0^{2\pi} I_1(\phi') \, e^{jkb_1 \sin \theta \cos(\phi - \phi')} \sin \phi' d\phi' \tag{26}$$

$$A_{1y}^r = \frac{b_1 \mu}{4\pi} \frac{e^{-jkr_o}}{r_o} \int_0^{2\pi} I_1(\phi') \, e^{jkb_1 \sin \theta \cos(\phi - \phi')} \cos \phi' d\phi' . \tag{27}$$

The same procedure is followed to get the vector potential radiated by loop 2.

Equation (18) is substituted into equations (26) and (27). The resulting integrals are solved as follows:

$$I_{1_n}(o) = -\frac{j}{\pi\zeta}\left[\frac{\begin{vmatrix} V_1 & \alpha_n^{12} \\ V_2 & \alpha_n^{22} \end{vmatrix}}{D_n}\right] \tag{28}$$

where $I_{1_n}(o)$ is the nth term in the series for loop 1 current at ϕ=o (the feed point) and $\zeta = \sqrt{\mu/e}$ where e is permittivity.

$$D_n = \alpha_n^{11}\,\alpha_n^{22} - \alpha_n^{12}\,\alpha_n^{21} \quad . \tag{29}$$

$$Q_{1_n} = \frac{b_1 \mu}{4\pi}\,\frac{e^{-jkr_o}}{r_o}\,I_{1_n}(1) \quad . \tag{30}$$

$$B_1 = kb_1 \sin\theta \quad . \tag{31}$$

Express $\sin\phi'$ and $\cos\phi'$ in exponential form so that

$$A^r_{1_{x_n}} = \frac{Q_{1_n}}{j2}\,(-K_a + K_b) \tag{32}$$

and

$$A^r_{1_{y_n}} = \frac{Q_{1_n}}{j2}\,(K_a + K_b) \tag{33}$$

where

$$K_a = \int_o^{2\pi} e^{j(n+1)\phi'}\, e^{jB_1\cos(\phi-\phi')}\, d\phi' \tag{34}$$

$$K_b = \int_o^{2\pi} e^{j(n-1)\phi'}\, e^{jB_1\cos(\phi-\phi')}\, d\phi' \quad . \tag{35}$$

These integrals are of the form of the Sommerfeld representation of the Bessel function:

$$J_n(B) = \frac{j^{-n}}{2\pi}\int_o^{2\pi} e^{jB\cos\Phi}\, e^{jn\Phi}\, d\Phi \quad . \tag{36}$$

Letting $\Phi = \phi - \phi'$ gives:

$$J_n(B) = \frac{j^{-n}}{2\pi} e^{-jn\phi} \int_{-\phi}^{2\pi-\phi} e^{jB\cos(\phi-\phi')} e^{jn\phi'} d\phi' . \tag{37}$$

This requires that

$$K_a = 2\pi\, j^{n+1}\, e^{j(n+1)\phi}\, J_{n+1}^{(B_1)} . \tag{38}$$

and

$$K_b = 2\pi\, j^{n-1}\, e^{j(n-1)\phi}\, J_{n-1}^{(B_1)} . \tag{39}$$

The components of the vector potential due to the component $I_{1_n}^{(\phi)}$ in spherical coordinates are:

$$A_{1_{\theta_n}}^r = (A_{1_{x_n}}^r \cos\phi + A_{1_{y_n}}^r \sin\phi)\cos\theta \tag{40}$$

and

$$A_{1_{\phi_n}}^r = (-A_{1_{x_n}}^r \sin\phi + A_{1_{y_n}}^r \cos\phi) . \tag{41}$$

Substituting (30), (34), and (35) into (40) and (41) gives:

$$A_{1_{\theta_n}}^r = \frac{jQ_{1_n}}{2} [(K_a - K_b)\cos\phi - j(K_a + K_b)\sin\phi]\cos\theta \tag{42}$$

$$= \frac{jQ_{1_n}}{2} [K_a e^{-j\phi} - K_b e^{j\phi}]\cos\phi \tag{43}$$

$$A_{1_{\phi_n}}^r = \frac{Q_{1_n}}{2} [(K_a + K_b)\cos\phi - j(K_a - K_b)\sin\phi] \tag{44}$$

$$= \frac{Q_{1_n}}{2} (K_a e^{-j\phi} + K_b e^{j\phi}) . \tag{45}$$

Substitute (38) and (39) into (43) and (45) to get:

$$A_{1_{\theta_n}}^r = -\pi\, Q_{1_n}\, e^{jn(\phi+\pi/2)} [J_{n+1}^{(B_1)} + J_{n-1}^{(B_1)}]\cos\theta \tag{46}$$

$$= -2\pi\, Q_{1_n} e^{jn(\phi+\pi/2)} \frac{n}{B_1} J_n^{(B_1)} \cos\theta \tag{47}$$

and

$$A^r_{l_{\phi_n}} = -j\pi\, Q_{l_n}\, e^{jn(\phi+\pi/2)}\left[J_{n-1}(B_l) - J_{n+1}(B)\right] \tag{48}$$

$$A^r_{l_{\phi_n}} = -j2\pi\, Q_{l_n} e^{jn(\phi+\pi/2)}\, J'_n(B_l) \quad . \tag{49}$$

By summing all of the contributing vector potential components and using the recurrence relationships:

$$\frac{2n}{x} J_n(x) = J_{n+1}(x) + J_{n-1}(x)$$

and

$$2J'_n(x) = J_{n-1}(x) - J_{n+1}(x) \quad ,$$

the vector potential at a point due to loop l is:

$$A^r_{l_\theta} = \sum_{-\infty}^{\infty} A^r_{l_{\theta_n}} = -2\pi \sum_{-\infty}^{\infty} Q_{l_n}\, e^{jn(\phi+\frac{\pi}{2})}\, \frac{n}{B_l} J_n(B_l) \cos\theta \tag{50}$$

and

$$A^r_{l_\phi} = \sum_{-\infty}^{\infty} A^r_{l_{\phi_n}} = -j2\pi \sum_{-\infty}^{\infty} Q_{l_n}\, e^{jn(\phi+\pi/2)}\, J'_n(B_l) \quad . \tag{51}$$

Substitute $Q_l = \frac{-j\mu}{4\pi^2\zeta} \frac{b_l e^{-jkr_o}}{r_o}$ into equations (50) and (51).

$$A^r_{l_\theta} = -2\pi\, Q_l \sum_{-\infty}^{\infty} \frac{\begin{vmatrix} V_1 & \alpha_n^{12} \\ V_2 & \alpha_n^{22} \end{vmatrix}}{D_n} e^{jn(\phi+\frac{\pi}{2})} \frac{n}{kb_l} \frac{J_n(kb_l \sin\theta)}{\sin\theta} \cos\theta \quad . \tag{52}$$

$$A^r_{l_\phi} = -j2\pi\, Q_l \sum_{-\infty}^{\infty} \frac{\begin{vmatrix} V_1 & \alpha_n^{12} \\ V_2 & \alpha_n^{22} \end{vmatrix}}{D_n} J'_n(kb_l \sin\theta) \quad . \tag{53}$$

Since $\alpha^{ii}_{-n} = \alpha^{ii}_n$ and $J_{-n}(x) = (-1)^n J_n(x)$, equations (52) and (53) can be rewritten as:

$$A^r_{1_\theta} = -2\pi\, Q_1 \sum_1^n n \frac{\begin{vmatrix} V_1 & \alpha_n^{12} \\ V_2 & \alpha_n^{22} \end{vmatrix}}{D_n} \frac{J_n(kb_1 \sin\theta)}{kb_1 \sin\theta} \cos\theta$$

$$\cdot\left[e^{jn(\phi+\pi/2)} - (-1)^n e^{-jn(\phi+\pi/2)}\right] . \tag{54}$$

and

$$A^r_{1_\phi} = -j2\pi\, Q_1 \left\{ \frac{\begin{vmatrix} V_1 & \alpha_o^{12} \\ V_2 & \alpha_o^{22} \end{vmatrix}}{D_o} J_o'(kb_1 \sin\theta) + \sum_1^n \frac{\begin{vmatrix} V_1 & \alpha_n^{12} \\ V_2 & \alpha_n^{22} \end{vmatrix}}{D_n} J_n'(kb_1 \sin\theta) \right.$$

$$\left. \cdot\left[e^{jn(\phi+\pi/2)} + (-1)^n e^{-jn(\phi+\pi/2}\right] \right\} . \tag{55}$$

The electromagnetic field from loop 1 is then given by:

$$\epsilon^r_1 = -j\omega(\hat{\theta}\, A^r_{1_\theta} + \hat{\Phi}\, A^r_{1_\phi}) . \tag{56}$$

King shows that for a single loop of moderate size, $|kb| \leq 2.5$, the significant contributions are from the first three terms of the series [7].

The electric field patterns for the ϕ and θ modes for loop 1 are readily obtained using the first three terms of the respective series. The identities:

$$J_o'(x) = -J_1(x)$$

and

$$J_1'(x) = J_o(x) - \frac{J_1(x)}{x}$$

are used.

n=0:

$$A^r_{1\theta_o} = 0; \quad A^r_{1\phi_o} = j2\pi\, Q_1 \frac{\begin{vmatrix} V_1 & \alpha_o^{12} \\ V_2 & \alpha_o^{22} \end{vmatrix}}{D_o} J_1(kb_1 \sin\theta) \tag{57}$$

$$\varepsilon^r_{1o} = \hat{\phi}\, E^r_{1\phi_o} = 2\pi\, Q_1\, \omega \frac{\begin{vmatrix} V_1 & \alpha_o^{12} \\ V_2 & \alpha_o^{22} \end{vmatrix}}{D_o} J_1(kb_1 \sin\theta) \tag{58}$$

(Note that for the constant current distribution situation the series has only the n=0 term.)

n=1:

$$A^r_{1\theta_1} = 4\pi\, Q_1 \frac{\begin{vmatrix} V_1 & \alpha_1^{12} \\ V_2 & \alpha_1^{22} \end{vmatrix}}{D_1} \frac{J_1(kb_1 \sin\theta)}{kb_1 \sin\theta} \cos\theta \sin\phi \tag{59}$$

$$A^r_{1\phi_1} = 4\pi\, Q_1 \frac{\begin{vmatrix} V_1 & \alpha_1^{12} \\ V_2 & \alpha_1^{22} \end{vmatrix}}{D_1} J_1'(kb_1 \sin\theta) \cos\phi \tag{60}$$

$$\varepsilon^r_{11} = \hat{\theta}\, E^r_{1\theta_1} + \hat{\Phi}\, E_{1\phi_1} \tag{61}$$

$$E^r_{1\theta_1} = -j4\pi\, Q_1 \omega \frac{\begin{vmatrix} V_1 & \alpha_1^{12} \\ V_2 & \alpha_1^{22} \end{vmatrix}}{D_1} \frac{J_1(kb_1 \sin\theta)}{kb_1 \sin\theta} \cos\theta \sin\phi \tag{62}$$

$$E^r_{1\phi_1} = -j4\pi\, Q_1 \omega \frac{\begin{vmatrix} V_1 & \alpha_1^{12} \\ V_2 & \alpha_1^{22} \end{vmatrix}}{D_1} J_1'(kb_1 \sin\theta) \cos\phi \tag{63}$$

n=2:

$$A^r_{1\theta_2} = j4\pi\, Q_1 \frac{\begin{vmatrix} V_1 & \alpha_2^{22} \\ V_2 & \alpha_2^{22} \end{vmatrix}}{D_2} \frac{2J_2(kb_1 \sin\theta)}{kb_1 \sin\theta} \cos\theta \sin 2\phi \tag{64}$$

$$A^r_{1\phi_2} = j4\pi\, Q_1\, e^{j2\phi}\, \frac{\begin{vmatrix} V_1 & \alpha_2^{12} \\ V_2 & \alpha_2^{22} \end{vmatrix}}{D_2}\, J_2'(kb_1 \sin\theta)\cos 2\phi \tag{65}$$

$$\varepsilon^r_{1_2} = \hat{\theta}\, E^r_{1_{\theta_2}} + \hat{\phi}\, E^r_{1_{\phi_2}} \tag{66}$$

$$E^r_{1_{\theta_2}} = (4\pi\, Q_1 \omega)\, \frac{\begin{vmatrix} V_1 & \alpha_2^{12} \\ V_2 & \alpha_2^{22} \end{vmatrix}}{D_2}\, \frac{2J_2(kb_1 \sin\theta)}{kb_1 \sin\theta}\, \cos\theta \sin 2\phi \tag{67}$$

$$E^r_{1_{\phi 2}} = (4\pi\, Q_1 \omega)\, \frac{\begin{vmatrix} V_1 & \alpha_2^{12} \\ V_2 & \alpha_2^{22} \end{vmatrix}}{D_2}\, J_2'(kb_1 \sin\theta)\cos 2\phi \tag{68}$$

The field from loop 2 is found in the same manner. To find the total field at a point for each mode, each term of the series for loop 2 for both modes is multiplied by the phase factor, exp (jkc cosθ) to account for the separation of the loops. The total electric fields for the ϕ mode and θ mode are expressed as follows:

$$\varepsilon^r_\theta = E^r_{1_{\phi_o}} + E^r_{2_{\phi_o}} e^{jkc\cos\theta} + E^r_{1_{\phi_1}} + E^r_{2_{\phi_1}} e^{jkc\cos\theta}$$

$$+ E^r_{1_{\phi_2}} + E^r_{2_{\phi_2}} e^{jkc\cos\theta}$$

and

$$\varepsilon^r_\theta = E^r_{1_{\theta_o}} E^r_{2_{\theta_o}} e^{jkc\cos\theta} + E^r_{1\theta_1} + E^r_{2_{\theta_1}} e^{jkc\cos\theta}$$

$$+E^r_{1_{\theta_2}} + E^r_{2_{\theta_2}} e^{jkc\cos\theta} \quad .$$

The gain of the array is calculated by dividing the square of the field by the power radiated. Where:

$$\text{Power Radiated} = P_{rad} = V_1^2 \cdot Y_{IN_1} + V_2^2 \cdot Y_{IN_2} \quad . \tag{69}$$

In order to find the input admittance, it is necessary to first derive expressions for self and mutual admittance. By treating the two coupled loops like the two-port network in Figure 4, equations (70) and (71) can be written directly:

$$I_1(o) = Y_{11} V_1 + Y_{12} V_2 \tag{70}$$

$$I_2(o) = Y_{21} V_1 + Y_{22} V_2 \quad . \tag{71}$$

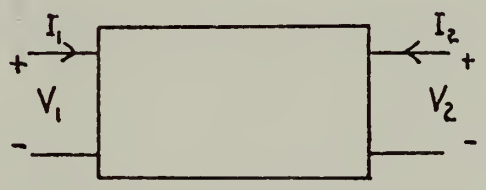

Figure 4. Two-Port Network

$I_1(o)$ and $I_2(o)$ are the feedpoint currents. Because the network is reciprocal, $Y_{12} = Y_{21}$. Solving for mutual admittance:

$$Y_{12} = \frac{I_1(o)}{V_2}\bigg|_{V_1=o} = \frac{1}{j\Pi n_o}\left[\frac{-\alpha_o^{12}}{D_o} + 2\sum_{n=1}^{\infty}\frac{-\alpha n^{12}}{D_n}\right]\bigg|_{V_2=1} \quad . \tag{72}$$

Self-admittance is by definition:

$$Y_{11} = \frac{I_1(o)}{V_1}\bigg|_{V_2=0} \tag{73}$$

$$Y_{22} = \frac{I_2(o)}{V_2}\bigg|_{V_1=0} \quad . \tag{74}$$

The input admittance is by definition:

$$Y_{IN_1} = \frac{I_1}{V_1} = Y_{11} + \frac{V_2}{V_1} Y_{12} \tag{75}$$

$$Y_{IN_2} = \frac{I_2}{V_2} = Y_{22} + \frac{V_2}{V_1} Y_{21} \quad . \tag{76}$$

In order to simplify the digital computer program used later in solving for the electric field and gain, it will be assumed that both driving voltages are purely real. This will allow Y_{IN} to be replaced by G_{IN} where G_{IN} equals the real part of Y_{IN}.

Then:

$$G_{IN_1} = G_{11} + \frac{V_2}{V_1} G_{12} \tag{77}$$

and

$$G_{IN_2} = G_{22} + \frac{V_1}{V_2} G_{21} \quad . \tag{78}$$

Finally,

$$Gain_\phi = \frac{\left| E^r_{1\phi} + E^{r'}_{2\phi} \right|^2}{P_{rad}} \tag{79}$$

and:

$$Gain_\theta = \frac{\left| E^r_{1\theta} + E^{r'}_{2\theta} \right|}{P_{rad}} \tag{80}$$

$E^{r'}_{2\phi}$ and $E^{r'}_{2\theta}$ represent $E^r_{2\phi}$ and $E^r_{2\theta}$ respectively multiplied by the phase factor ($e^{+jkc\cos\theta}$) which accounts for effects of loop separation.

III. DISCUSSION OF NUMERICAL TECHNIQUES AND COMPUTER PROGRAM

The α_n^{ij} terms were computed on an IBM System/360 Model 67 digital computer in FORTRAN IV language using Adler's basic program [1]. Beyond this point the programming was straight forward. Flow charts on Figures 5a, 5b, and 5c show the major steps in the program. The flow chart of Figures 5a and 5b is for computing $I_1(\phi)$, $I_2(\phi)$, Y_{s1}, Y_{s2}, Y_{11}, Y_{22}, and Y_{12} where Y_{s1} and Y_{s2} are the self admittance of loops 1 and 2 respectively with mutual coupling effects ignored. Figures 5a and 5c show the steps in computing Gain_ϕ and Gain_θ. The computer results for current in the isolated loop were compared with King's [8], while the gain was compared with the work of Harrington and Mautz [4]. In both cases the agreement was exact. The incrementing of parameters b and c in the program allows for changing loop size and loop spacing. Incrementing θ and ϕ allow for computation of gain patterns.

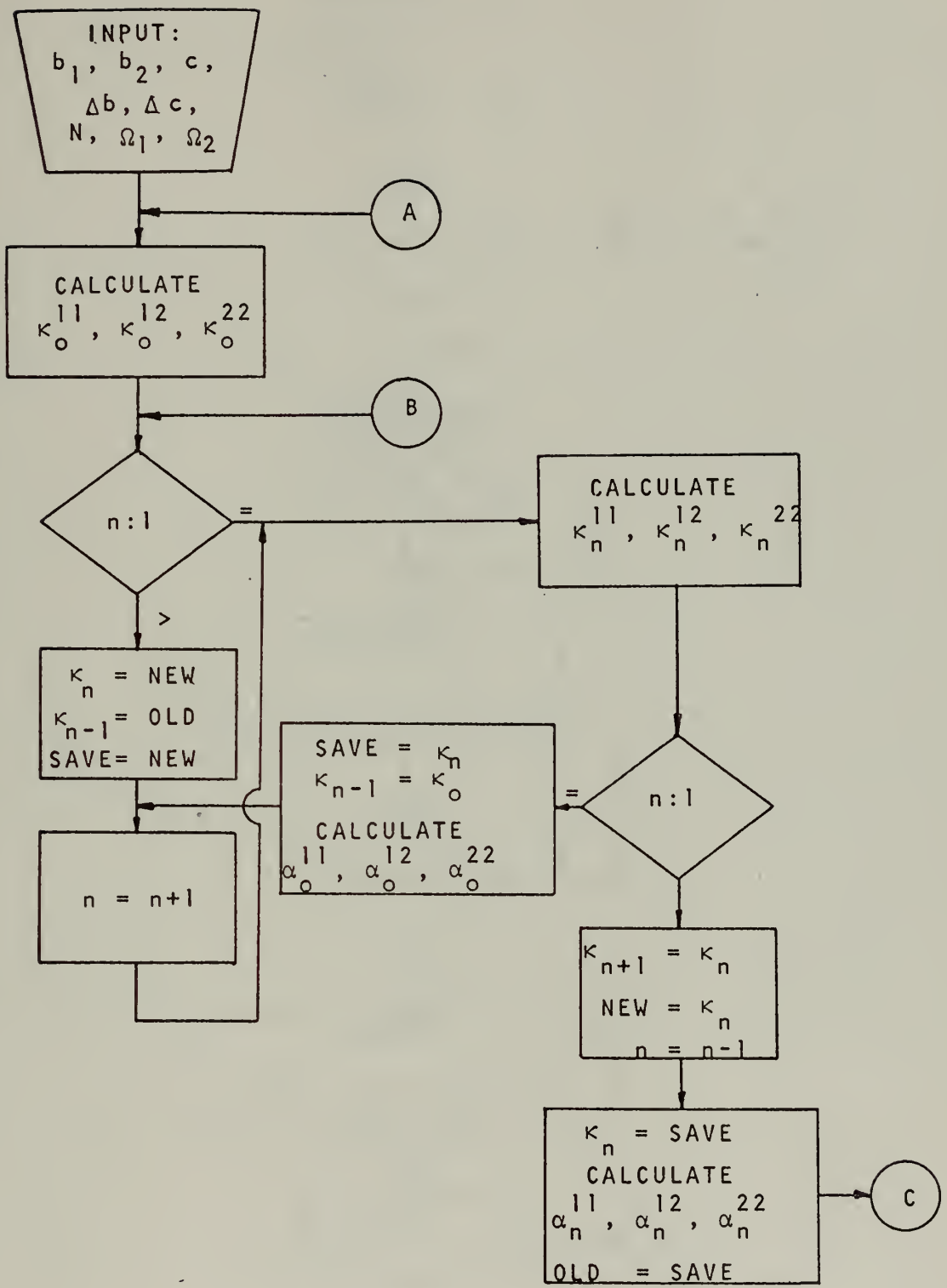

Figure 5a. Flow Chart of Computer Program

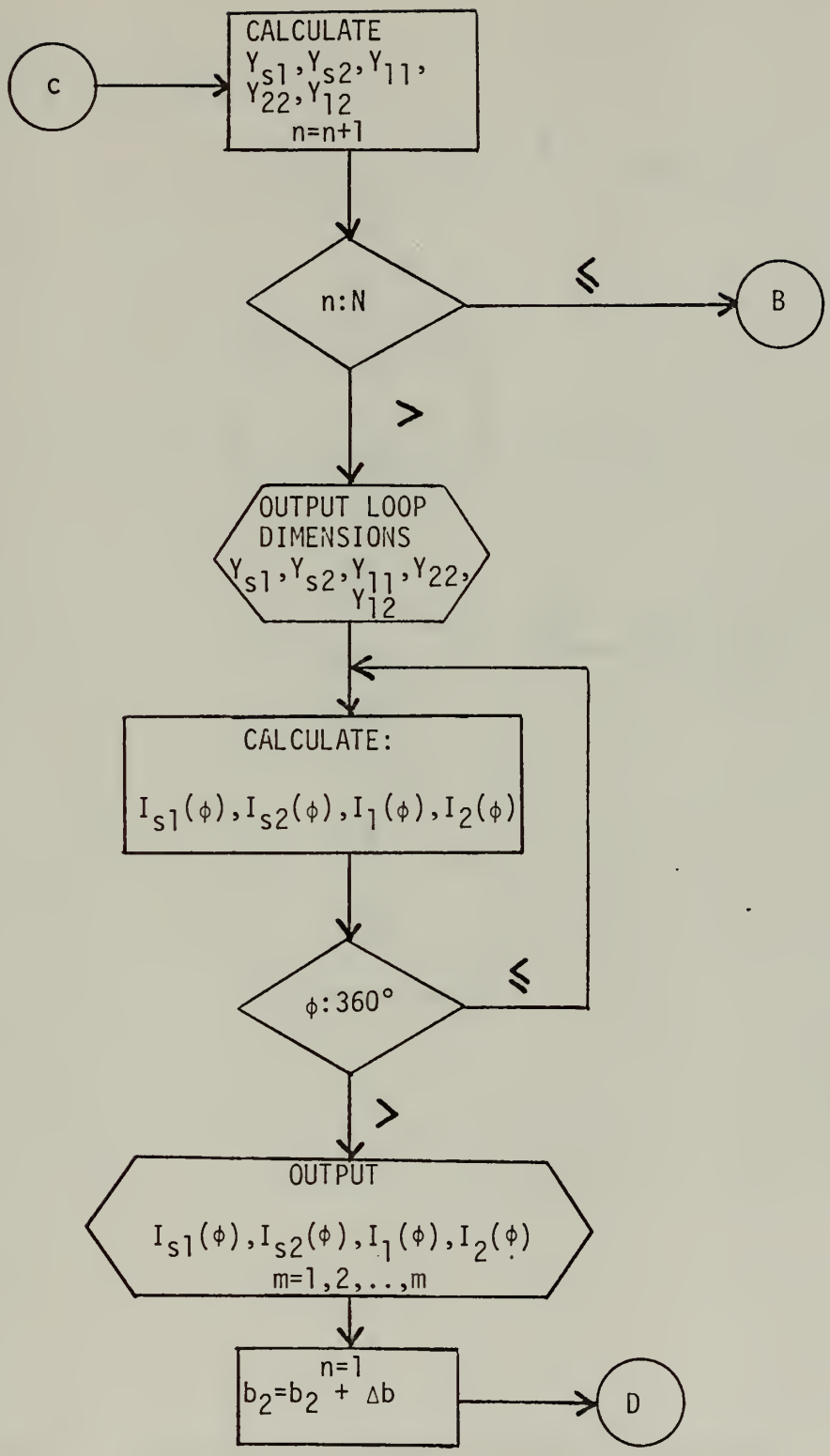

Figure 5b. Flow Chart of Computer Program

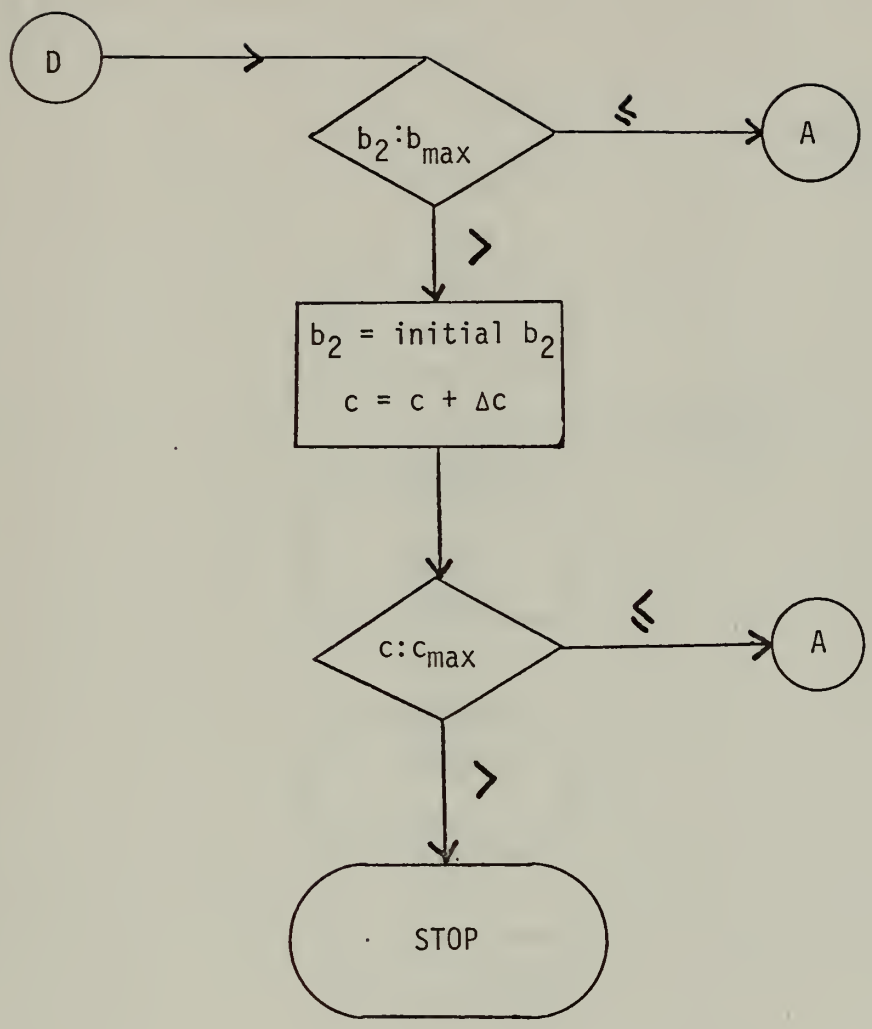

Figure 5b. Flow Chart of Computer Program (Continued)

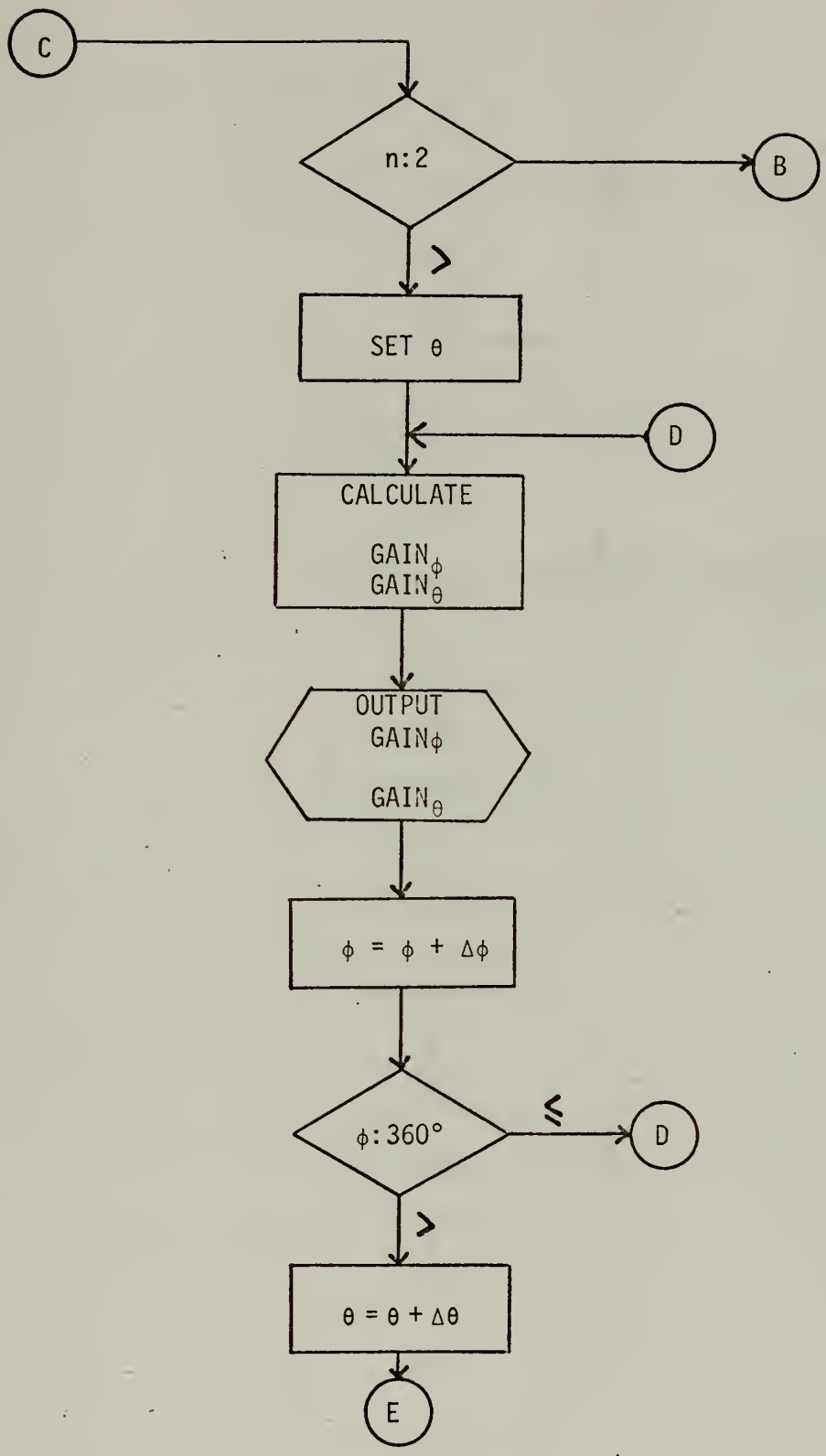

Figure 5c. Flow Chart of Computer Program

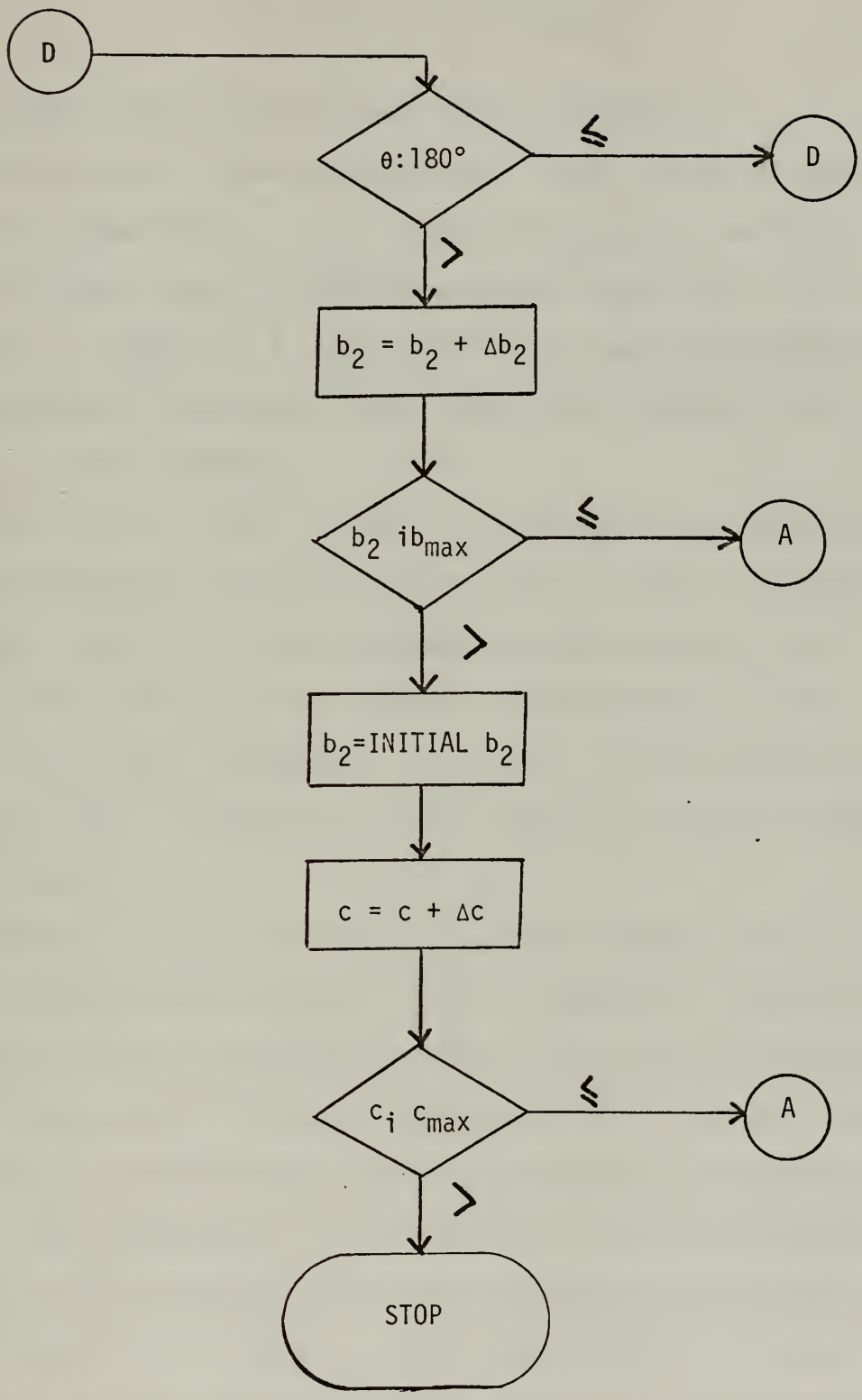

Figure 5c. Flow Chart of Computer Program (Continued)

IV. DISCUSSION OF RESULTS

A. CURRENT DISTRIBUTION AND GAIN PATTERN CORRELATION

Figures 6 and 7 show the patterns of $Gain_\phi$ in the x-z plane and the x-y plane respectively. In all cases presented $kb_1=1$ and loop 1 is in the x-y plane. Loop 2 is positioned coaxially above loop 1 at a distance c. Figures 8, 9, 10, 11 and 12 show the corresponding current distributions for the case of both loops driven in phase by one volt delta function generators.

For $.5 \leq kc \leq 1$ and $.5 \leq kb_2 \leq 1.5$ the radiation patterns do not change significantly and only a slight change in phase of loop 2 current is noted. When $kc > 1$ radical changes in pattern shapes occur. This shows that as the separation becomes larger than about $\lambda/6$, the effect of the array factor predominates. When $kb_2 = .5$ the circumference of loop 2 is $\lambda/2$. In this case the loop supports a 1/2 cycle standing current wave.

Figures 13 and 14 are the $Gain_\phi$ patterns in the x-z and x-y planes respectively, for the case when loop 2 is parasitic. Figures 15, 16, 17, and 18 are the corresponding plots of the current distributions. When the two loops are closely coupled, $kc = .5$ and resonant the currents are large and almost equal in magnitude but 180 degrees out of phase. Even though $Gain_\phi$ is relatively high in this configuration, the benefit of large currents is not realized because of the phase difference between the two currents. As the separation of the loops is increased from approximately $\lambda/13$ to approximately $\lambda/6$, the currents drop by a factor of about five; however, the $Gain_\phi$ drops only slightly.

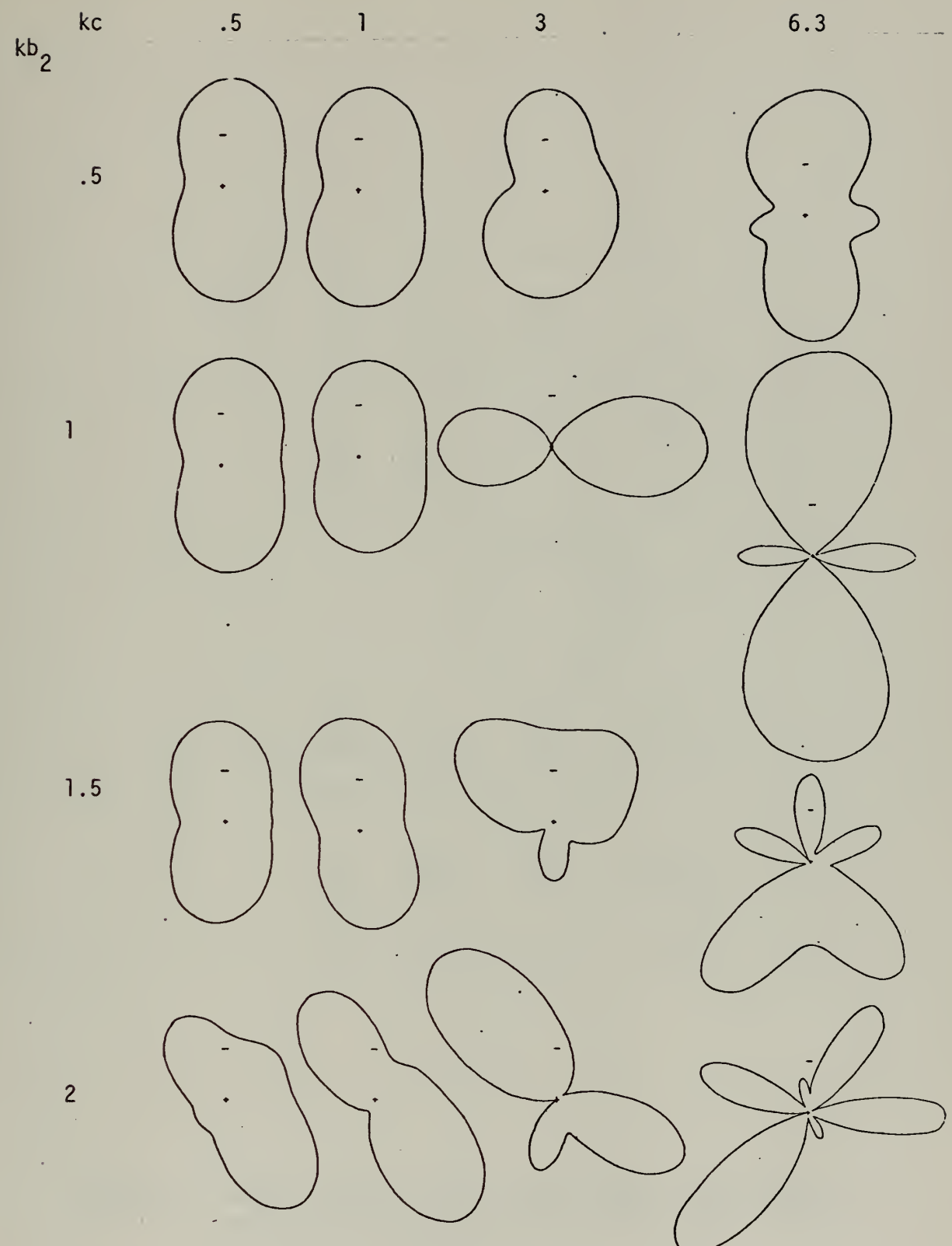

Figure 6. Gain ϕ patterns in x-z plane (ϕ= o°,180°); feed point at ϕ=o°, θ=90°; ϕ=o° at right, θ=o° at top; Ω=10, kb_1=1, $V_1=V_2=1$; kc=.5,1,3,6.3; kb_2 = .5,1,1.5,2.

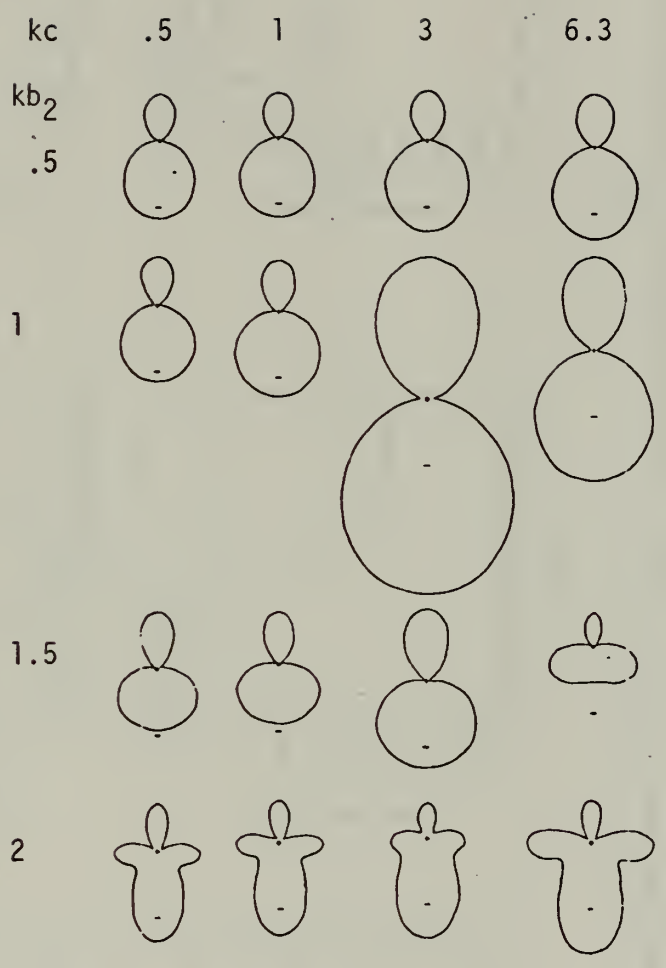

Figure 7. Gain ϕ patterns in X-Y plane, θ=90°; feed point at bottom (ϕ=0°); Ω=10, kb_1=1, V_1=V_2=1; kc = .5,1,3, 6.3; kb_2 = .5,1,1.5,2.

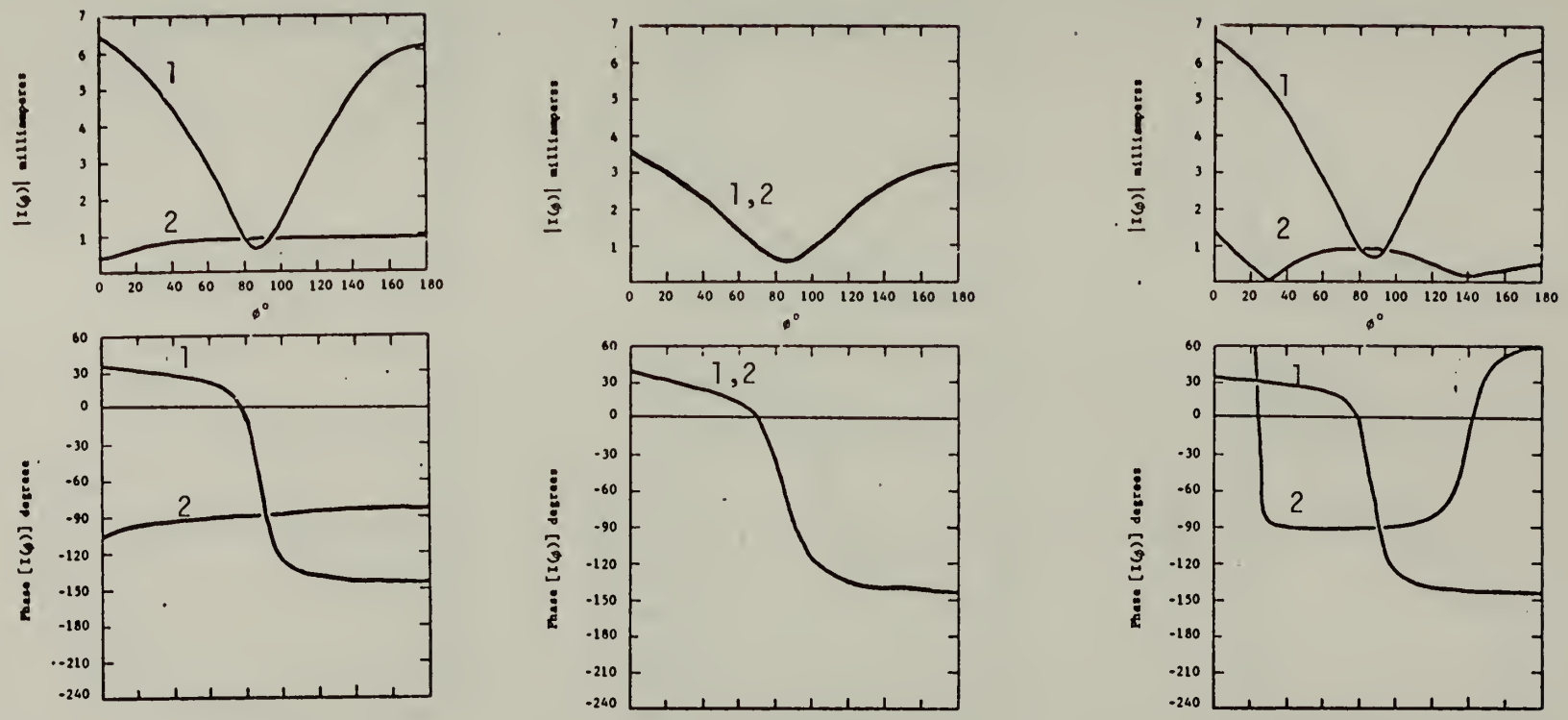

Figure 8. Magnitude and phase for loops 1 and 2 current distributions for Ω=15, $V_1=V_2=1$, $kb_1=1$, kc=.5; (a) $kb_2=.5$; (b) $kb_2=1$; (c) $kb_2=1.5$.

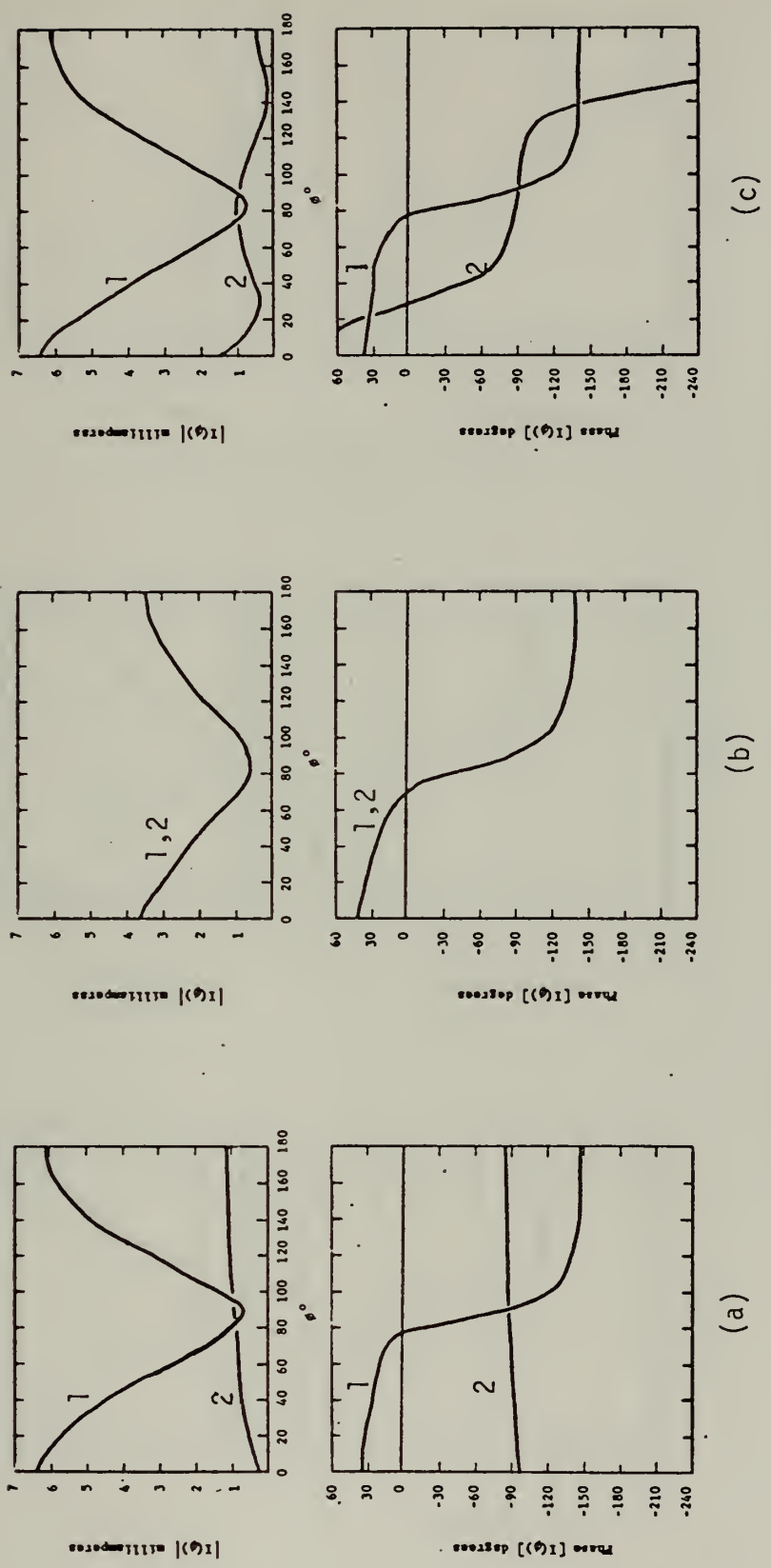

Figure 9. Magnitude and phase for loops 1 and 2 current distributions for Ω= 15, $V_1=V_2=1$, $kb_1=1$, kc=1; (a) $kb_2=.5$; (b) $kb_2=1$; (c) $kb_2=1.5$.

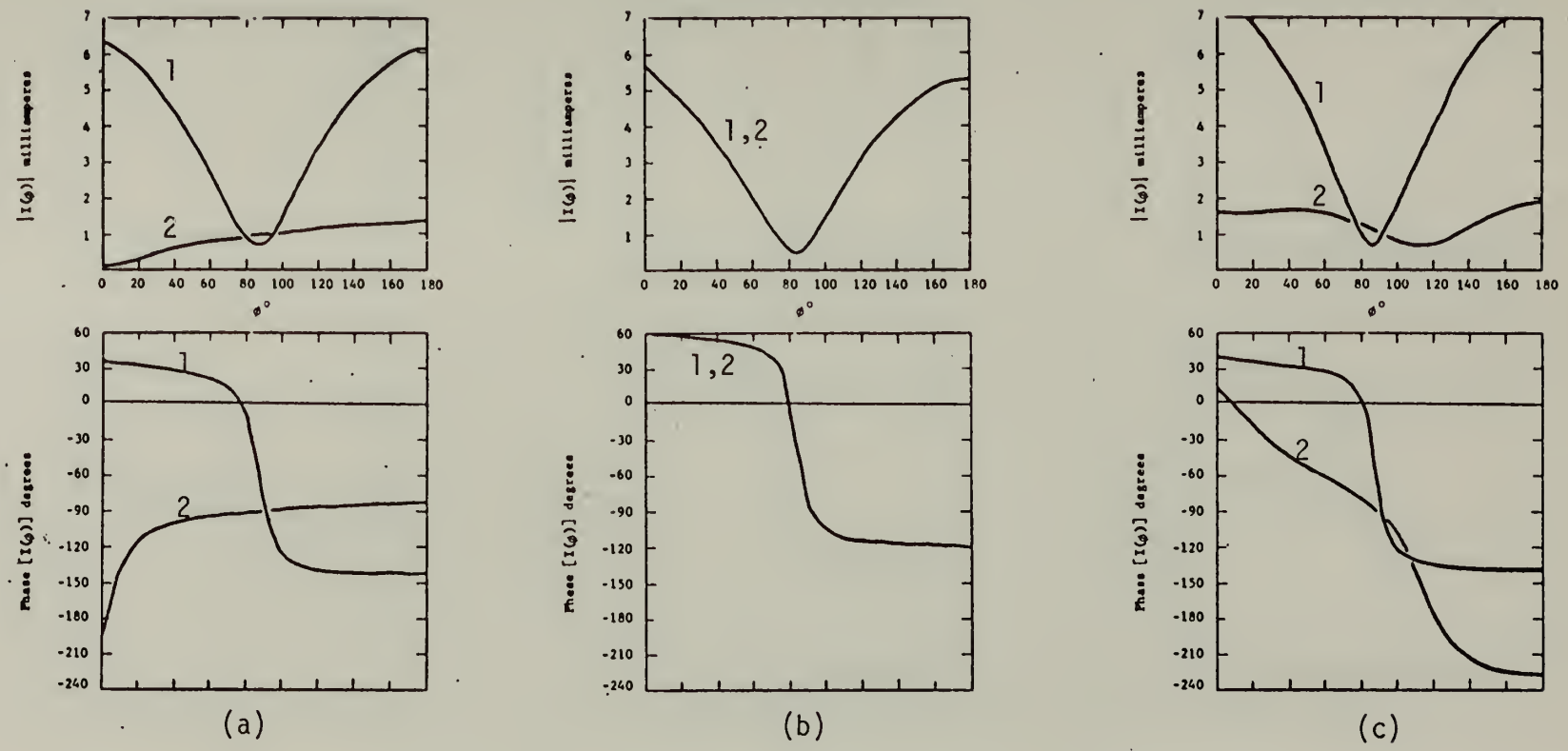

Figure 10. Magnitude and phase for loops 1 and 2 current distributions for Ω= 15, $V_1=V_2=1$, $kb_1=1$, kc=3; (a) $kb_2=.5$; (b) $kb_2=1$; (c) $kb_2=1.5$.

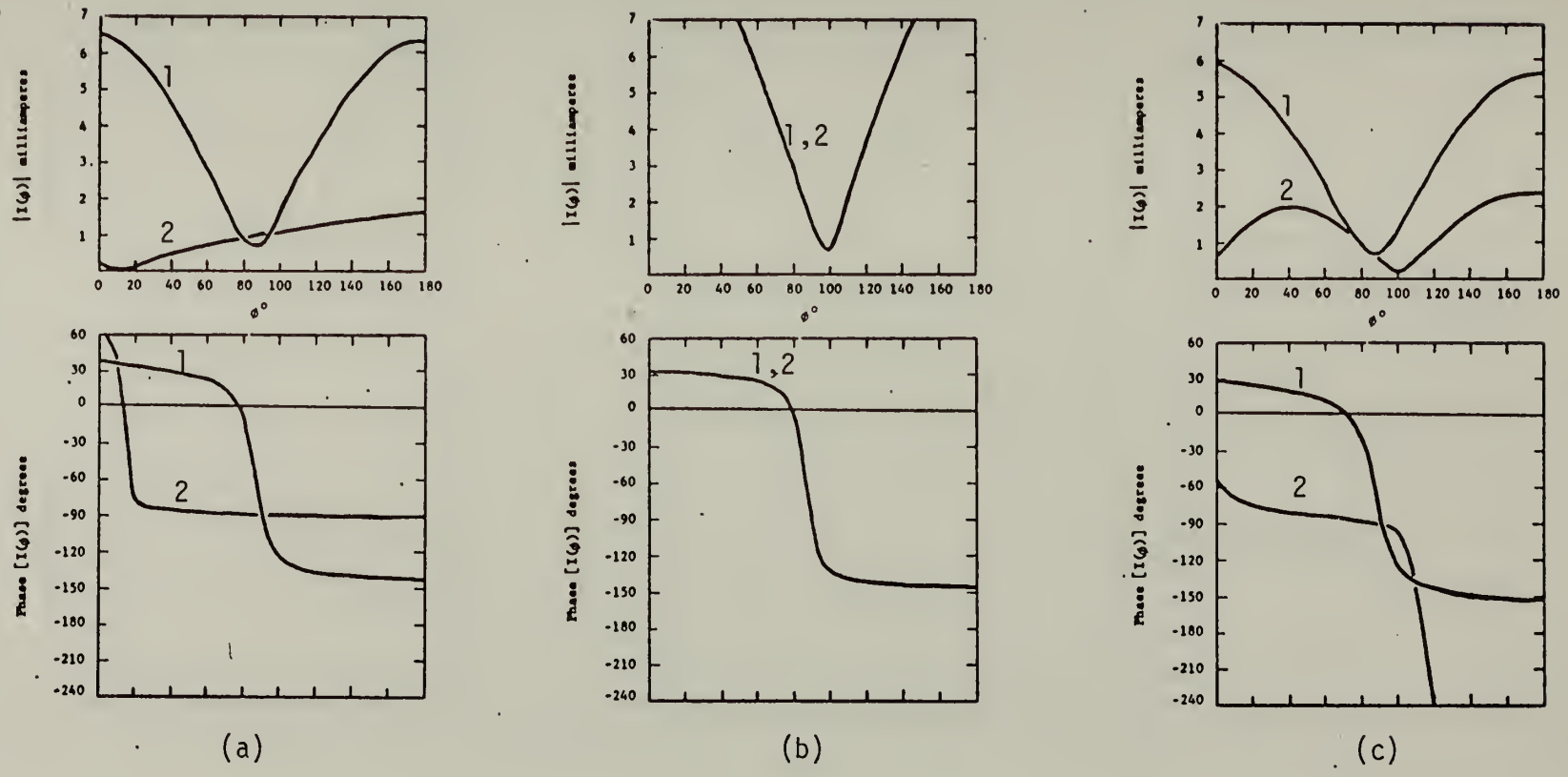

Figure 11. Magnitude and phase for loops 1 and 2 current distributions for Ω=15, kc=5, V_1=V_2=1, kb=1, (a) kb_2 = .5; (b) kb_2 = 1; (c) kb_2 = 1.5.

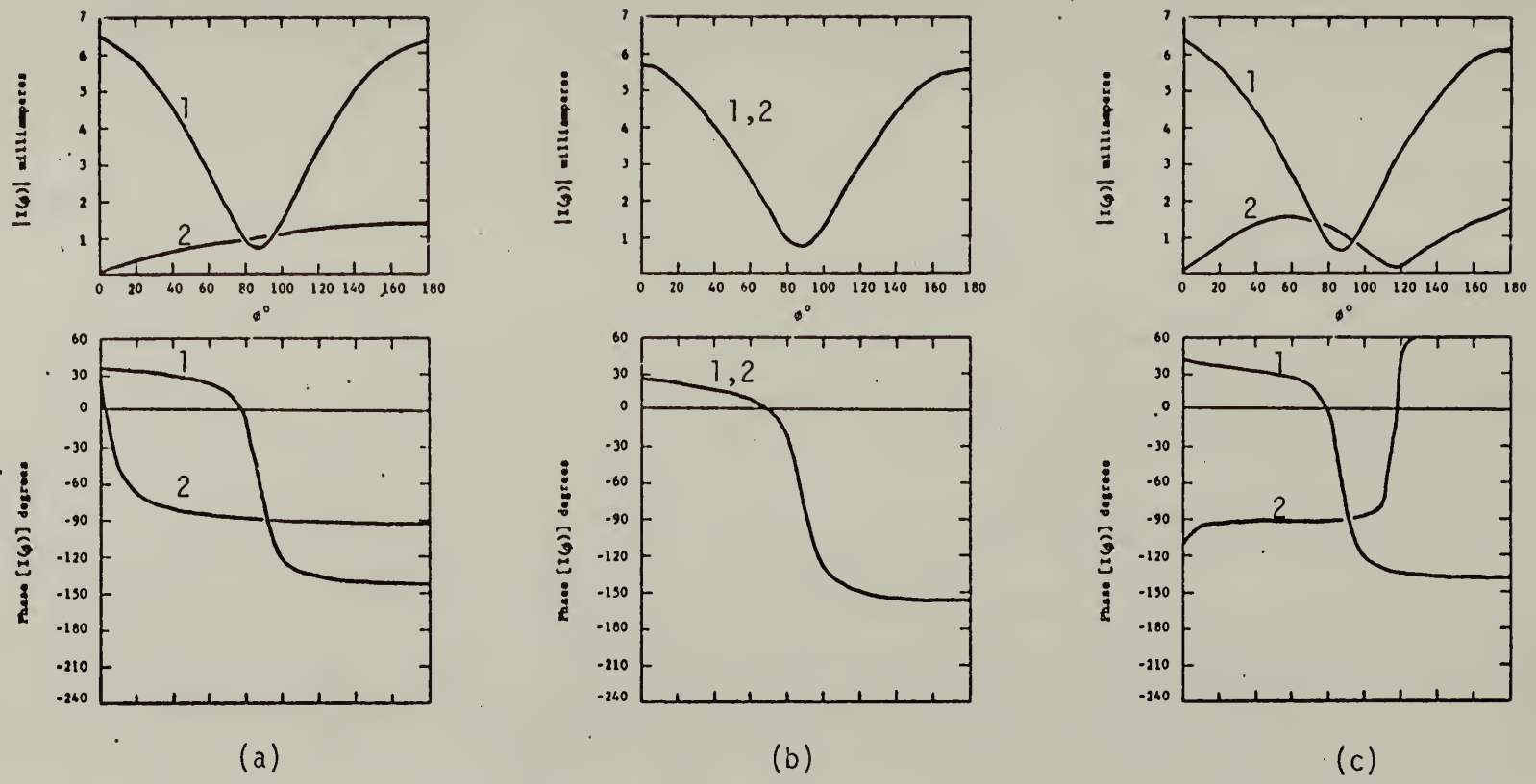

Figure 12. Magnitude and phase for loops 1 and 2 current distributions for Ω=15, V_1=V_2=1, kb_1=1, kc=7; (a) kb_2=.5; (b) kb_2=1; (c) kb_2=1.5.

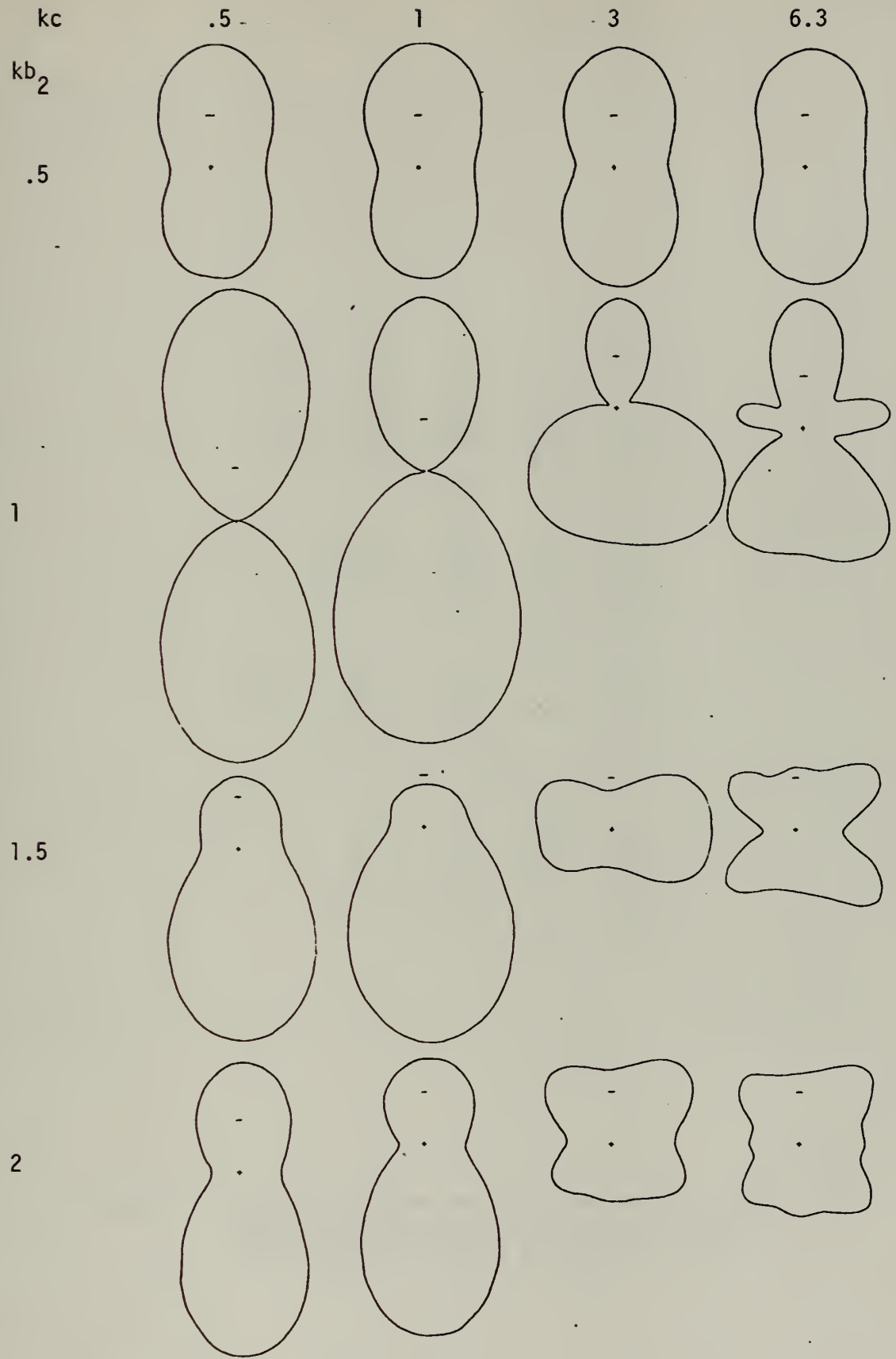

Figure 13. Gain ϕ patterns in X-Z plane (ϕ=o°,180°); feed point at ϕ=o°, θ=90°, ϕ=o° at right, θ=o° at top; Ω=10, kb_1=1, V_1=1, V_2=0; kc=.5,1,3,6.3; kb_2=.5,1,1.5,2.

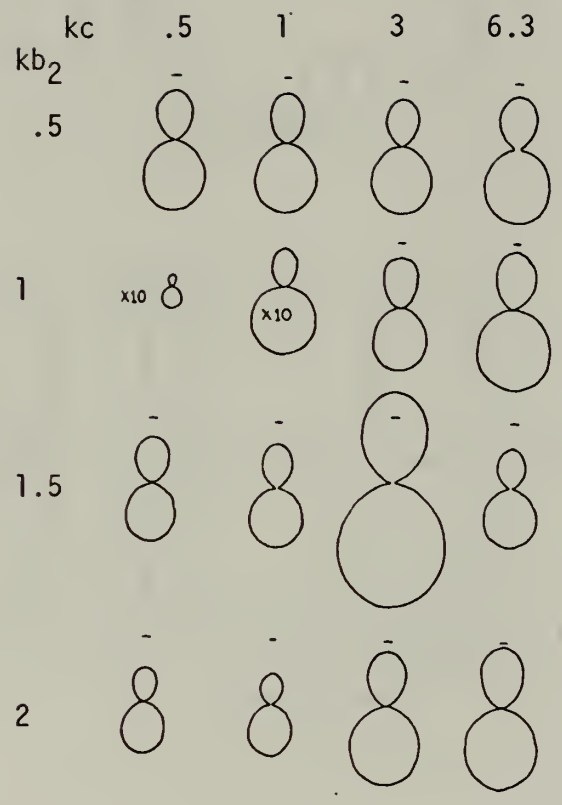

Figure 14. Gain ϕ patterns in X-Y plane, θ=90°; feed point at bottom (ϕ=0°; Ω=10, V_1=1, V_2=0, kb_1=1; kc=.5,1,3,6.3; kb_2=.5,1,1.5,2.

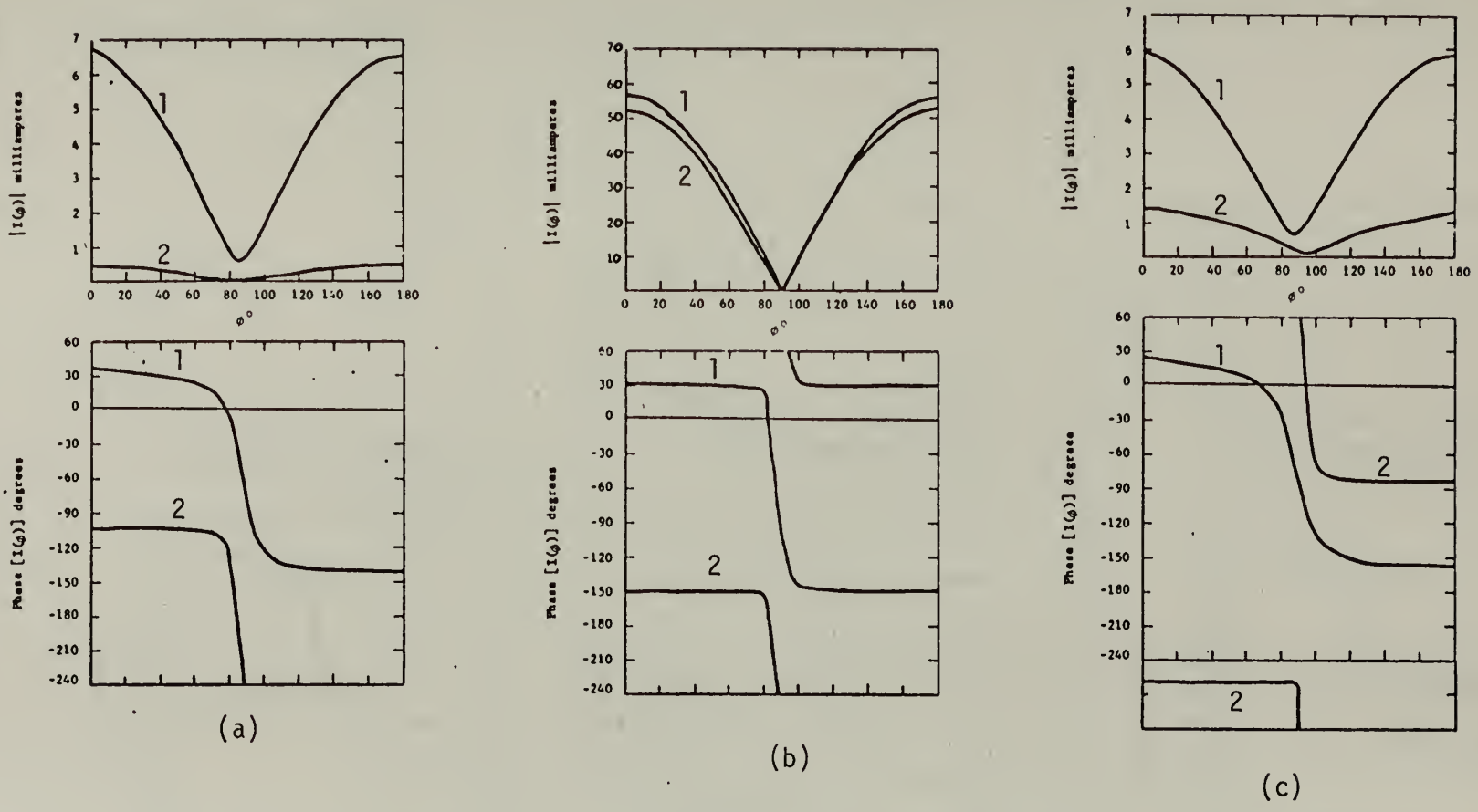

Figure 15. Magnitude and phase for loops 1 and 2 current distributions for Ω=15, V_1=1, V_2=0, kb_1=1, kc=.5; (a) kb_2=.5; (b) kb_2=1; (c) kb_2=1.5.

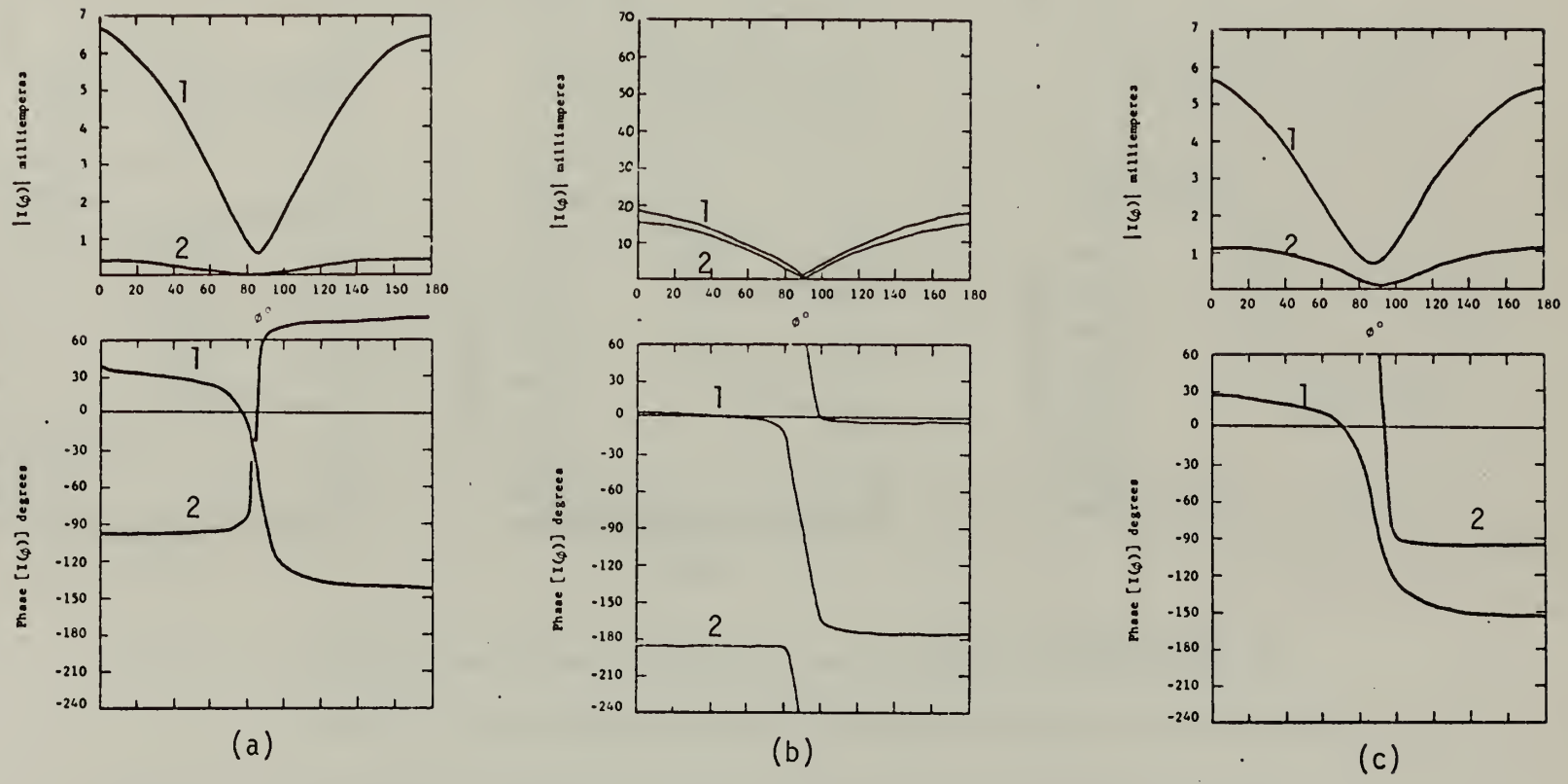

Figure 16. Magnitude and phase for loops 1 and 2 current distributions for Ω=15, V_1=1, V_2=0, kb_1=1, kc=1; (a) kb_2=.5; (b) kb_2=1; (c) kb_2=1.5.

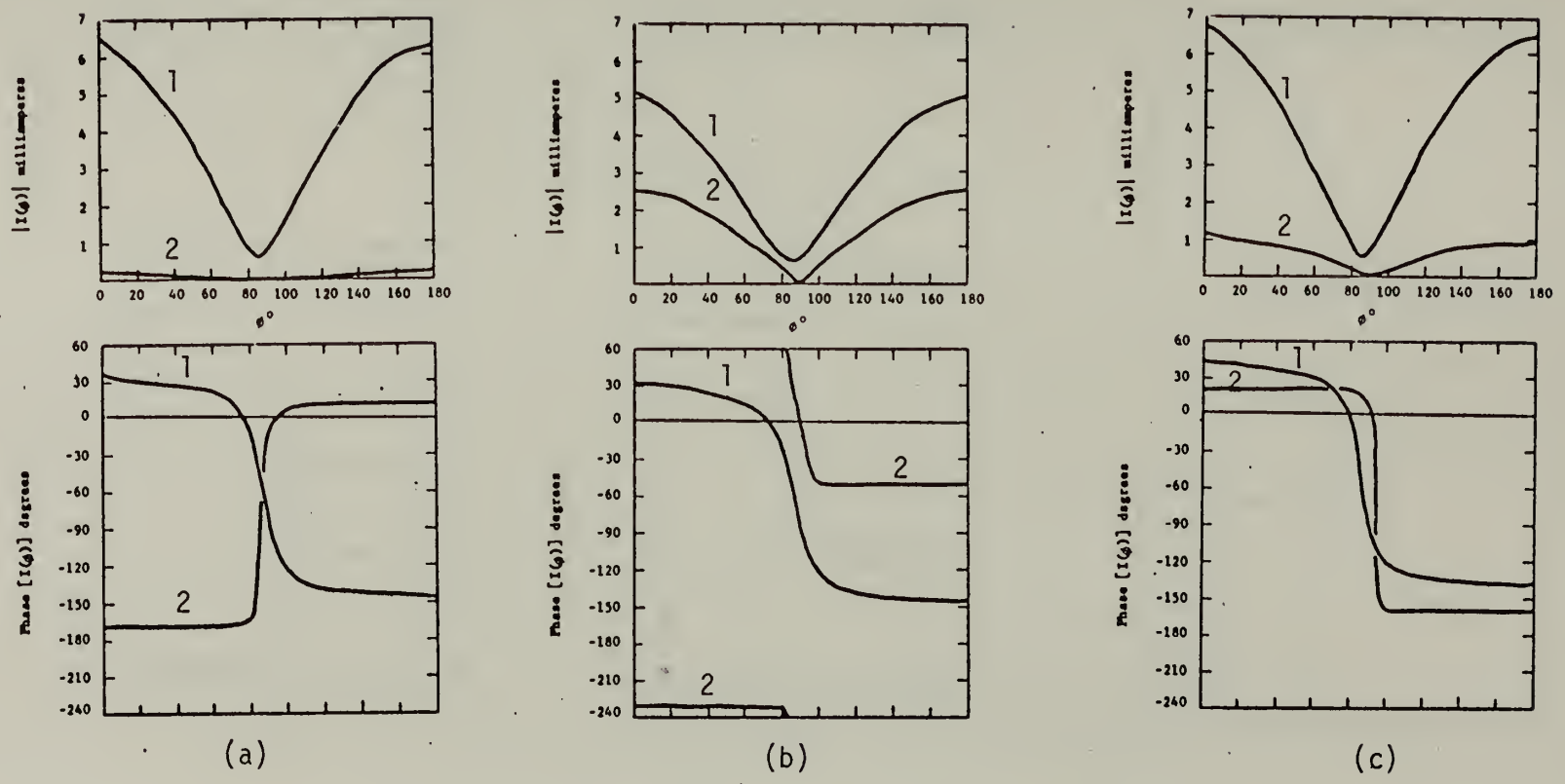

Figure 17. Magnitude and phase for loops 1 and 2 current distributions for Ω=15, V_1=1, V_2=0, kb_1=1, kc=3; (a) kb_2=.5; (b) kb_2=1; (c) kb_2=1.5.

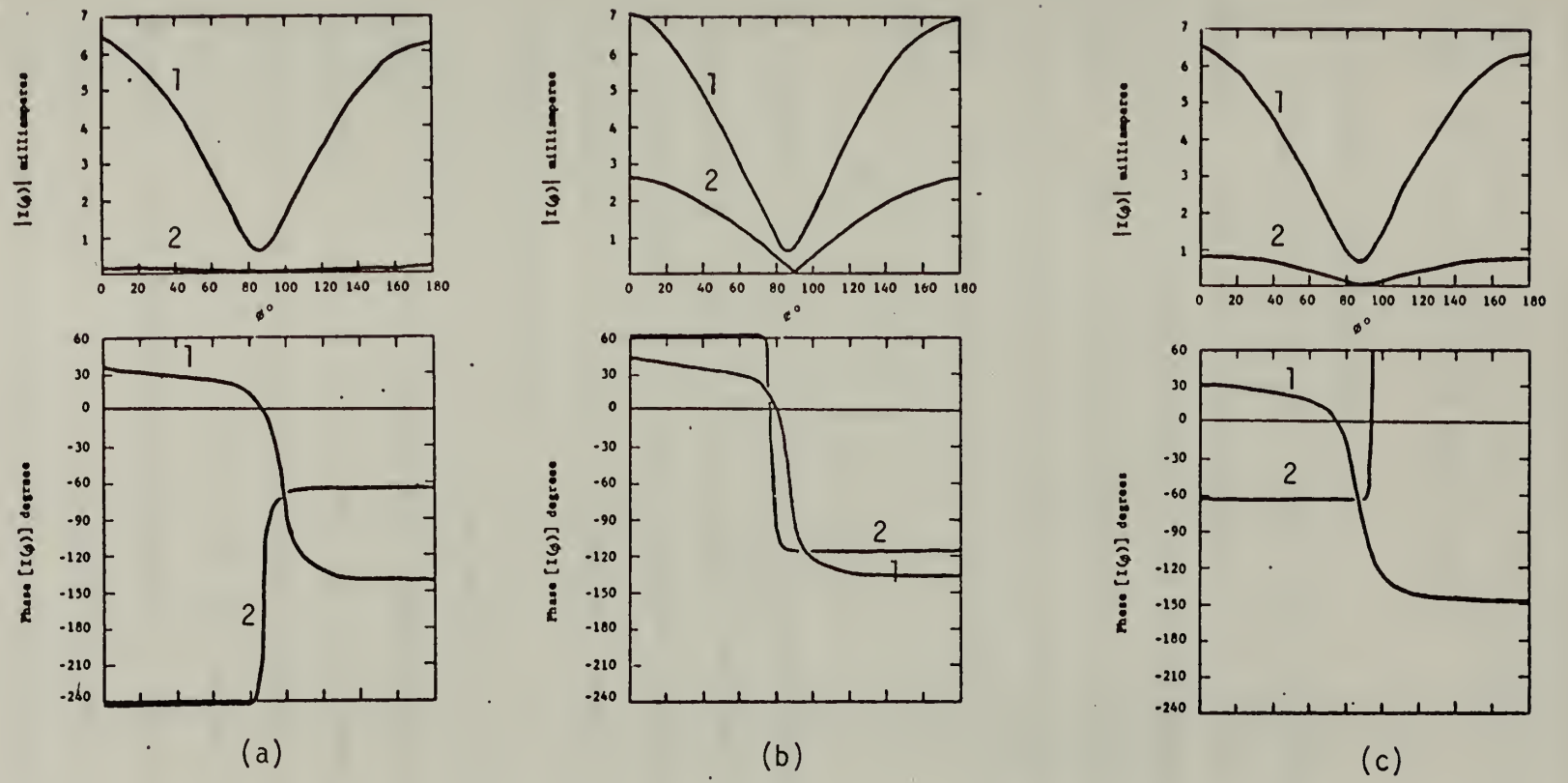

Figure 18. Magnitude and phase for loops 1 and 2 current distributions for Ω =15, V_1=1, V_2=0, kb_1=1, kc=4.5; (a) kb_2=.5; (b) kb_2=1; (c) kb_2=1.5.

This observation is explained as follows: although the currents are much smaller when $c \simeq \lambda/6$, the phases of the two currents are no longer exactly opposing. This in turn allows the total vector potential of the ϕ mode in both cases to be almost equal.

B. CURRENT DISTRIBUTIONS

Referring again to the current plots, the following observations are made. When both loops are resonant and driven, the current peak increases as c increases from $\lambda/12$ to λ and decreases as c increases beyond λ. When c is increased beyond 2λ (not shown) the mutual coupling is negligible and the loop currents are very close to those of isolated loops. This phenomenon is due to the behavior of the input admittance, where:

$$Y_{IN_1} = Y_{11} + Y_{12} \Big|_{V_1 = V_2 = 1.}$$

By computing Y_{11}, Y_{22}, Y_{12} and $Y_{IN_{1,2}}$ the following was noted: (a) with close coupling Y_{12} has a large negative real part which approaches zero as c is increased; (b) the real part of Y_{11} is always positive; (c) Y_{IN} increases as c increases. Therefore, since $I(0) = Y_{IN}V$, the current increases as Y_{IN} increases.

Of particular interest is the behavior of the current in the parasitic loop. In all cases both resonant and non-resonant the magnitude of the parasitic current, although reduced, paralleled the magnitude of the current on the driven resonant loop. In the resonant case when the spacing was close, the two currents were 180 degrees out of phase, but as the spacing approached λ, the currents approached the in-phase condition. Also in the parasitic case the phases of both currents tend to be constant with an abrupt reversal at the nulls.

C. GAIN PATTERNS

Figures 6 and 7, the $Gain_\phi$ patterns in the x-z plane and x-y plane respectively are again referred to. In these figures Ω=10, V_1=V_2=1 volt, kb_1=1, kc=.5, 1, 3 and 6.3 from left to right, while kb_2=.5, 1, 1.5 and 2 from top to bottom. In all patterns presented "+" marks the antenna center and "⌒" marks unity gain. With kb_2 fixed, the patterns are seen to change shape as kc increases from .5 to 6.3. This is due in small measure to the change in mutual coupling and primarily to the array factor. The smallest $Gain_\phi$ in the z direction occurs at kb_1 = kb_2 = 1 and kc = 3 ($c \simeq \lambda/2$); the largest $Gain_\phi$ in the z direction occurs also with the resonant array but with kc = 6.3 ($c \simeq \lambda$). In the former case the vector potentials were nearly 180 degrees out of phase and in the latter both vector potentials were in phase. In the extreme case where kb_2 = 2 and kc = 6.3, lobing occurs due to the combination of the array factor and the diverse current distributions on the two loops.

$Gain_\phi$ for the parasitic case is illustrated by Figures 13 and 14. The higher gains and more interesting patterns are attained in this configuration. As would be expected, less lobing now occurs and the parasitic element functions as a reflector. Of special interest are the kb_2 = 1.5, kc = 1 and kb_2 = 2, kc = 6.3 patterns. In the first of these particular arrangements the loop array pattern resembles that of a log periodic antenna. Figure 21 shows the effect of changing kb_2 to 1.2 and varying kc from .6 to 1.2. When kb_2 = kc = 1.2 the antenna is unidirectional. In contrast to this configuration, note the resulting pattern when kb_2 = 2 and kc = 6.3. The pattern is almost square with the gain across the top nearly uniform. Figure 14 shows a section of

these same patterns in the X-Y plane. These patterns closely resemble those of the familiar single-loop pattern in shape.

The effect of changing the b/a ratio is illustrated in Figure 19. The change in Ω is from 7.5 to 15, which represents a b/a ratio change of about 10 to 300. Although the effect is measurable, it is concluded that the loop array is not sensitive to changes in Ω.

Figure 20 shows the consequence of ignoring the mutual coupling when calculating the gain pattern (the dotted curves are with coupling ignored). In Figure 20a ($kc = .5$ and $kb_1 = kb_2 = 1$) the coupling is very significant, but as seen in Figures 20b and 20c ($kc = 6.3$, $kb_2 = 1$ and 1.5 respectively) the coupling has little effect.

Sample patterns of $Gain_\theta$ are shown in Figure 22. Although significant, this mode is certainly of secondary importance.

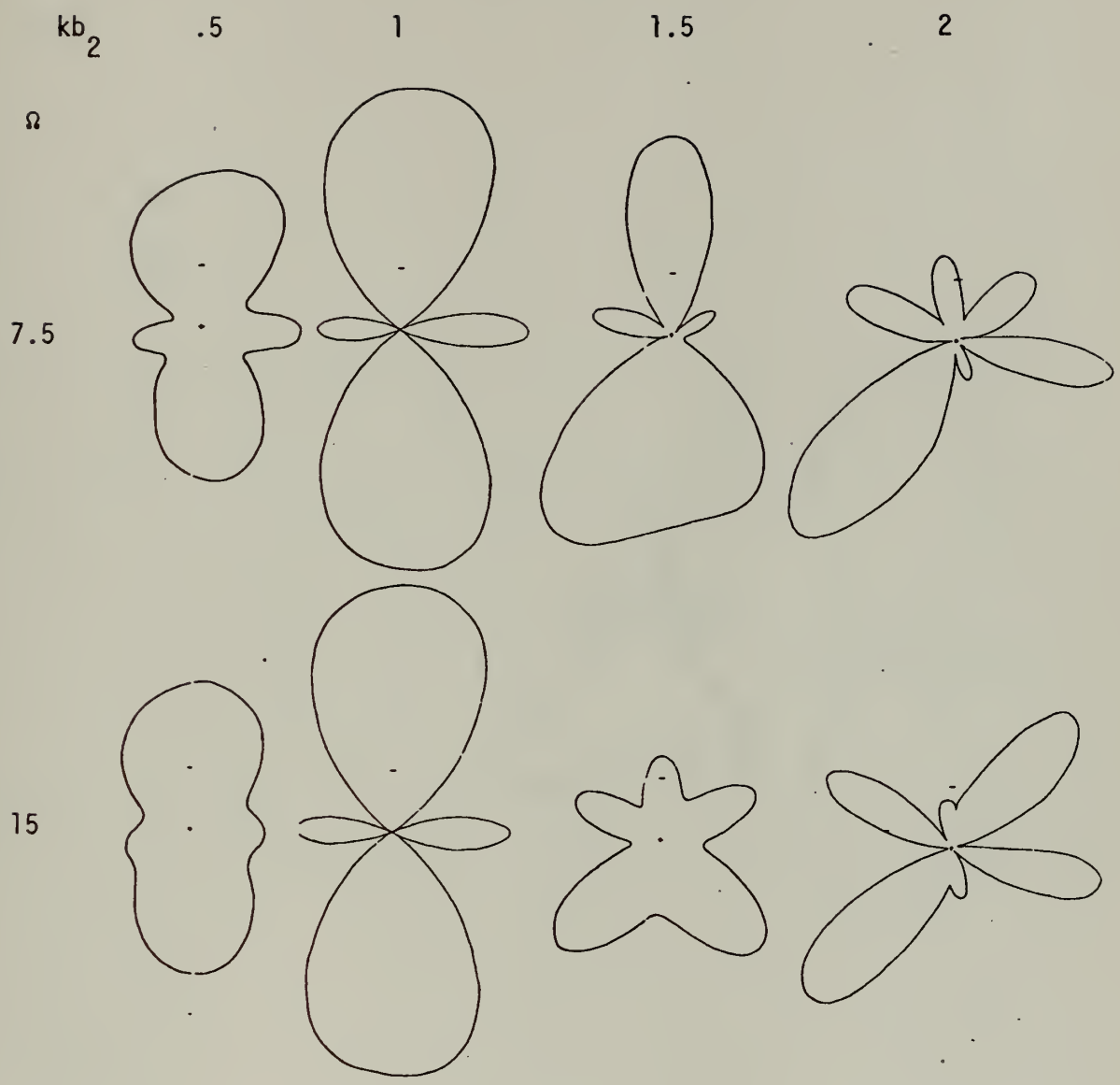

Figure 19. Gain ϕ patterns in X-Z plane (ϕ=o°,180°) for $V_1=V_2=kb_1=1$, kc=6.3; kb_2=.5,1,1.5,2; Ω=7.5,15; ϕ=o° at right, θ=o° at top.

kc	.5	6.3	6.3
kb_2	1	1.5	1

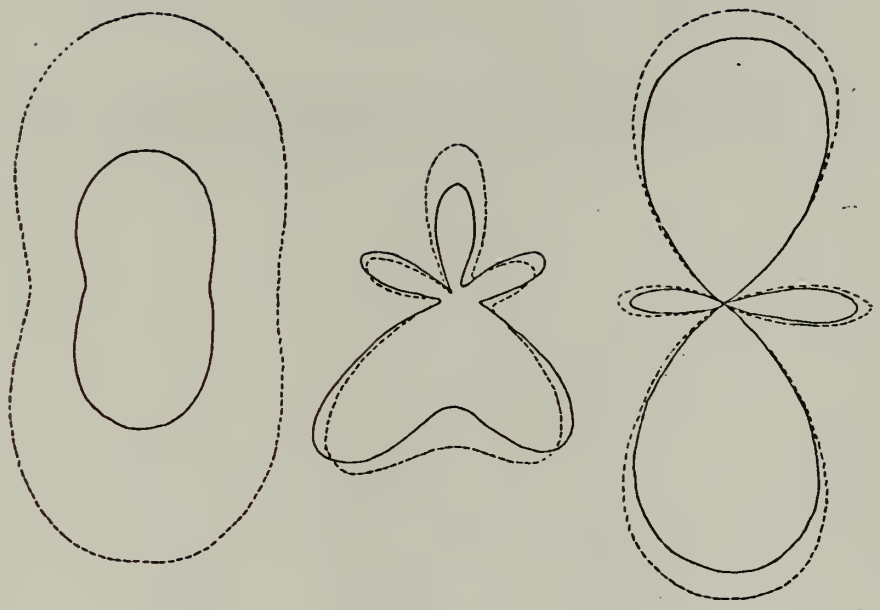

Figure 20. Gain ϕ patterns in X-Z plane with (solid lines) and without (dotted lines) mutual coupling effects. Ω=10, kb_1=1, ϕ=o° at right, θ=o° at top.

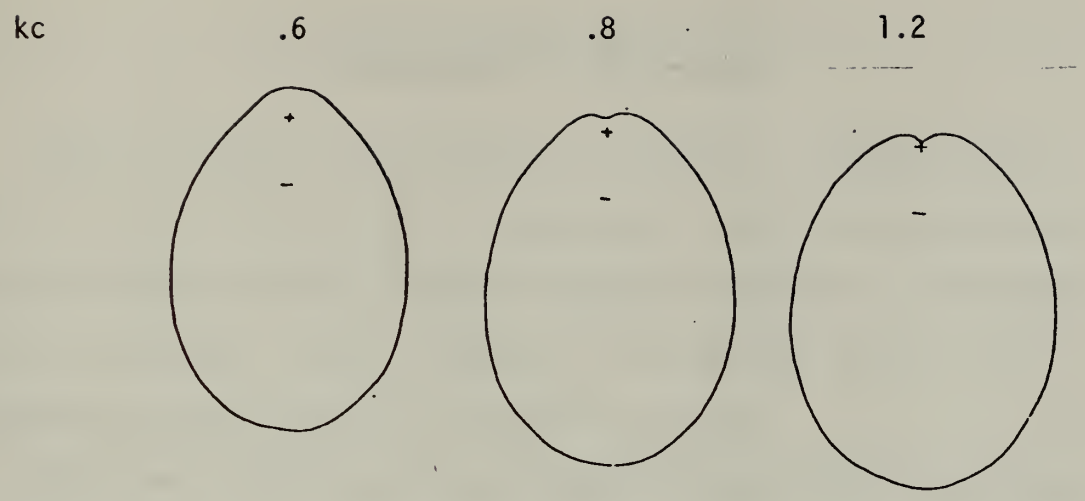

Figure 21. Gain ϕ patterns in X-Z plane (ϕ=o°,180°) for =10, V_1=1, V_2=o, kb_1=1, kb_2=1.2, kc=.6,.8,1.2.

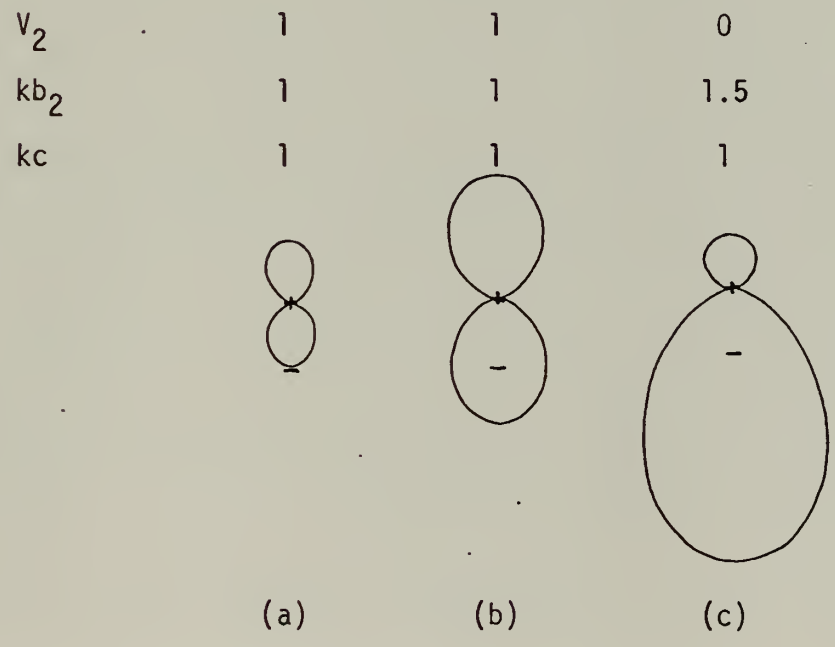

Figure 22. Gain θ patterns for Ω=10, kb_1=1 in (a) ϕ=45°, 225° plane; (b) ϕ=90°, 270°; (c) ϕ=90°, 270°.

V. SUGGESTIONS FOR FURTHER STUDY

Since this study is of a theoretical nature an immediate requirement is to confirm the results by experiment. First the current distributions and next the field intensity patterns for various arrangements should be measured. Also of interest in the two loop array is the consequence of open circuiting the parasitic loop.

The current and gain equations then should be solved for the three element case. Of interest would be the consequence of arranging three or more elements to make a log periodic loop antenna.

APPENDIX A

Evaluation of Fourier Coefficients κ_n^{ij}

Case I: $i = j$

Combining equations (5) and (15) results in:

$$\kappa_n^{ii} = \frac{1}{(2\pi)^2} \int_{-\pi}^{\pi} \int_{-\pi}^{\pi} e^{jn\theta} \frac{e^{-jkR_{ii}}}{R_{ii}} \, d\psi \, d\theta \tag{81}$$

By substituting $A_i = 2a_i \sin\frac{\psi}{2}$ in equation (81) and interchanging the order of integration one arrives at the expression:

$$\kappa_n^{ii} = \frac{2}{\pi} \int_0^{2a_i} \frac{M_n(A_i)}{\sqrt{4a_i^2 - A_i^2}} \, dA_i \tag{82}$$

where:

$$M_n(A_i) = \frac{1}{2\pi} \int_0^{\pi} e^{jn\theta} \frac{e^{-k R_{ii}}}{R_{ii}} \, d\theta; \; n \geq 0 \tag{83}$$

Storer showed that for the case of $A_i << b_i$:

$$b_1 M_n(A_i) = \frac{1}{\pi} \ln\left(\frac{8b_i}{A_i}\right) - \frac{2}{\pi} \sum_{m=1}^{n-1} \frac{1}{2m+1} - \frac{1}{2} \int_0^{2kb_i} [\Omega_{2n}(x) + j \, J_{2n}(x)] \, dx \tag{84}$$

where $\Omega_m(x)$ is the mth order Lommel-Weber function and $J_m(x)$ is the mth order cylindrical Bessel function of the first kind.

Wu devised an approximation method to evaluate equation (84) based on the facts that (a) the integral representation of:

$$\frac{1}{\pi} K_o \left\{ A_i \left(\frac{n^2}{b_i^2} - k^2 \right)^{\frac{1}{2}} \right\}$$

where $K_o(x)$ is the modified Bessel function of the second kind of zero order and the integral representation of $b_i M_n(A_i)$ are similar and (b) for A_i small the difference between $b_i M_n(A_i)$ and the small argument approximation for K_o is independent of A_i. The consequence of this is for moderate size n,

$$b_i M_n(A_i) = \frac{1}{2\pi} \left\{ 2K_o \left(A_i \sqrt{\frac{n^2}{b_i^2} - k^2} \right) + \ln \left(1 - \frac{k^2 b_i^2}{n^2} \right) \right\} +$$

$$2 C_n - \pi \int_o^{2kb_i} [\Omega_{2n}(x) + j J_{2n}(x)] \, dx \qquad (85)$$

where $C_n = \gamma - 2 \sum_{m=o}^{n-1} \frac{1}{2m+1} + \ln(4n)$ and γ is Euler's constant.

Because A_i is small, the K_o term in equation (85) can be slightly modified with a negligible loss in accuracy to:

$$K_o \left(A_i \sqrt{\frac{n^2}{b_i^2} - k^2} \right) \simeq K_o \left(\frac{nA_i}{b_i} \right) - \frac{1}{2} \left(\ln \quad 1 - \frac{k^2 b_i^2}{n^2} \right) \qquad (86)$$

By employing equations (85) and (86) equation (82) can be integrated to get:

$$\kappa_n^{ii} \simeq \frac{1}{2\pi b_i} \left\{ 2 K_o \left(\frac{na_i}{b_i} \right) I_o \left(\frac{na_i}{b_i} \right) + 2 C_n - \right. \qquad (87)$$

$$\left. \pi \int_o^{2kb_i} [\Omega_{2n}(x) + j J_{2n}(x)] \, dx \right\}$$

and:

$$\kappa_o^{ii} = \frac{1}{2\pi b_i} \left\{ \ln\left(\frac{8b_i}{a_i}\right) - \pi \int_o^{2kb_i} [\Omega_o^i(x) = j\, J_{2n}(x)]\, dx \right\} . \qquad (88)$$

Case II: $i \neq j$

By combining equation (15) with:

$$R_{ij} = [4b_i b_j \sin^2 (\tfrac{\phi-\phi'}{2}) + (b_i - b_j)^2 + c^2]^{\frac{1}{2}}$$

and

$$W_{ij}\,(\phi-\phi') = \frac{e^{-jkR_{ij}}}{R_{ij}}$$

equation (89) follows:

$$\kappa_n^{ij} = \frac{1}{2\pi} \int_{-\pi}^{\pi} \frac{e^{jn\phi} e^{-jk\,[4b_i b_j \sin^2 \frac{\phi}{2} + (b_i - b_j)^2 + c^2]^{\frac{1}{2}}}}{[4b_i b_j \sin^2 \frac{\phi}{2} + (b_i - b_j)^2 + c^2]^{\frac{1}{2}}}\, d\phi . \qquad (89)$$

It is necessary to solve equation (89) by numerical methods and the reader is referred to Adler's original work for the details of this process [1].

BIBLIOGRAPHY

1. Adler, R.W., The Mutual Admittance of Two Arbitrary Size Coaxial Circular Loop Antennas, Ph.D. Thesis, The Pennsylvania State University, The Graduate School, December 1970.

2. Collin, R.E. and Zucker, F.J., Antenna Theory, Part I, Ch.II, McGraw-Hill Book Company, New York, New York, 1969.

3. Hallen, E., Nova Acta Regiae Soc. Sci. Upsaliensis, Vol. 2, No.4, 1938.

4. Harrington, R.F. and Mautz, M.S., "Circular Wire Loops with Arbitrary Excitation and Loading," Proceedings of IEE, Vol.115, No.1, January 1968.

5. Iizuka,K., King, R.W.P., and Harrison, C.W.,Jr., "Self and Mutual Admittance of Two Identical Circular Loop Antennas in a Conducting Medium and in Air," IEEE Transactions on Antennas and Propagation, Vol. AP-L4, No.4, pp.440-449, July 1966.

6. Kennedy, P.A., "Loop Antenna Measurements," IRE Transactions on Antennas and Propagation, Vol. AP-4, pp.610-618, October 1956.

7. King, R.W.P., Harrison, C.W.,Jr., and Tingley,D.G. "The Admittance of Bare Circular Loop Antennas in a Dissipative Medium," IEEE Transactions on Antennas and Propagation, Vol.AP-12, pp.434-438, July 1964.

8. King, R.W.P., and Harrison, C.W., Jr., "Antennas and Waves: A Modern Approach," Ch.9, The M.I.T. Press, Massachusetts Institute of Technology, Cambridge, 1969.

9. Pocklington, H.C., Proceedings of the Cambridge Philosophical Society, Vol. 9, p.324, 1897.

10. Storer, J.E., "Impedance of Thin Wire Loop Antennas," Transactions of the AIEE, Vol.75, Part I, pp.606-619, November 1956.

11. Wu, T.T., "Theory of the Thin Circular Loop Antenna," Journal of Mathematical Physics, Vol.3, No.6, pp.1301-1304, November 1962.

INITIAL DISTRIBUTION LIST

		No Copies
1.	Defense Documentation Center Cameron Station Alexandria, Virginia 22314	2
2.	Library, Code 0212 Naval Postgraduate School Monterey, California 93940	2
3.	Asst. Professor Richard W. Adler, Code 52 Ab Department of Electrical Engineering Naval Postgraduate School Monterey, California 93940	3
4.	LCDR Joseph F. Corcoran, USN SMC# 2796 Naval Postgraduate School Monterey, California 93940	1

DOCUMENT CONTROL DATA - R & D

(Security classification of title, body of abstract and indexing annotation must be entered when the overall report is classified)

1. ORIGINATING ACTIVITY (Corporate author)
Naval Postgraduate School
Monterey, California 93940

2a. REPORT SECURITY CLASSIFICATION
Unclassified

2b. GROUP

3. REPORT TITLE
The Radiation Patterns and Current Distributions of Two Arbitrary Size Coaxial Circular Loop Antennas

4. DESCRIPTIVE NOTES (Type of report and, inclusive dates)
Master's Thesis; June 1971

5. AUTHOR(S) (First name, middle initial, last name)
Joseph Francis Corcoran

6. REPORT DATE
June 1971

7a. TOTAL NO. OF PAGES
59

7b. NO. OF REFS
11

8a. CONTRACT OR GRANT NO.

b. PROJECT NO.

c.

d.

9a. ORIGINATOR'S REPORT NUMBER(S)

9b. OTHER REPORT NO(S) (Any other numbers that may be assigned this report)

10. DISTRIBUTION STATEMENT
Approved for public release; distribution unlimited.

11. SUPPLEMENTARY NOTES

12. SPONSORING MILITARY ACTIVITY
Naval Postgraduate School
Monterey, California 93940

13. ABSTRACT

For many years the cylindrical dipole and circular loop have been thought of as the basic radiating elements. Due to its relative simplicity the study of the cylindrical dipole is quite complete, but owning to the degree of complexity, progress in the theory of the loop has been much slower. In recent years the isolated circular loop antenna of arbitrary size has been the subject of mathematical and experimental analysis [7], [6]. It was not until 1970 that the first complete and general mathematical solution for the mutual admittance of two arbitrary size coaxial circular loop antennas was published. The problem was formulated by Adler in terms of coupled integral equations for the current distributions on the loops [1]. The equations were solved using the Fourier series representation of the current distributions. The study presented here is the next logical step beyond the work of Adler. Using his current equations the current distributions are calculated. Radiation patterns and the loop current distributions are plotted for two cases: (1) both loops driven and (2) one loop acting as a short circuited parasite.

KEY WORDS	LINK A		LINK B		LINK C	
	ROLE	WT	ROLE	WT	ROLE	WT
Loop Antennas						

Thesis
C75462 Corcoran
c.1 The radiation patterns and current distributions of two arbitrary size coaxial circular loop antennas.
134929